

# Decision Potential Surface: A Theoretical and Practical Approximation of Large Language Model Decision Boundary

Zi Liang<sup>1</sup>, Zhiyao Wu<sup>2</sup>, Haoyang Shang<sup>3</sup>, Yulin Jin<sup>1</sup>, Qingqing Ye<sup>1</sup>, Huadi Zheng<sup>4</sup>,  
Peizhao Hu<sup>5</sup>, Haibo Hu<sup>1,6\*</sup>

<sup>1</sup>The Hong Kong Polytechnic University

<sup>2</sup>University of Macau

<sup>3</sup>Shanghai Jiaotong University

<sup>4</sup>Huawei

<sup>5</sup>Rochester Institute of Technology

<sup>6</sup>PolyU Research Centre for Privacy and Security Technologies in Future Smart Systems

{zi1415926.liang,yulin.jin}@connect.polyu.hk, bc31072@um.edu.mo

assassin808@sjtu.edu.cn, {qqing.ye,haibo.hu}@polyu.edu.hk

zhenghuadi@huawei.com, hxpvc@rit.edu

## Abstract

Decision boundary, the subspace of inputs where a machine learning model assigns equal classification probabilities to two classes, is pivotal in revealing core model properties and interpreting behaviors. While analyzing the decision boundary of large language models (LLMs) has attracted increasing attention recently, constructing it for mainstream LLMs remains computationally infeasible due to the enormous sequence-level output spaces and the autoregressive nature of LLMs. To address this issue, in this paper we propose *Decision Potential Surface (DPS)*, a new notion for analyzing the properties of LLM decisions. DPS is derived from the confidence in distinguishing different classes for each input, which naturally captures the *potential* of the decision boundary. We prove that the zero-height isohypse in DPS is equivalent to the decision boundary of an LLM, with enclosed regions representing decision regions. By leveraging DPS, for the first time in the literature, we propose a practical decision boundary approximation algorithm, namely  $K$ -DPS, which only requires only  $K$  finite sequence samples to approximate an LLM’s decision boundary with negligible error. We theoretically derive the upper bounds for the absolute error, expected error, and the error concentration between  $K$ -DPS and the ideal DPS, demonstrating that such errors can be traded off against sampling times.

## 1 Introduction

With the rapid advancement and remarkable success of large language models (LLMs), understanding their underlying mechanisms and behaviors has become increasingly critical (Wang et al. 2023; Conmy et al. 2023; Elhage et al. 2021; Ameisen et al. 2025; Sharkey et al. 2025; Allen-Zhu and Li 2025; Liang et al. 2025, 2024). A key approach to demystifying the “black box” of state-of-the-art AI models involves analyzing the *decision boundary* (Rosenblatt 1958), a fundamental concept for elucidating the characteristics of machine learning (ML) models. For LLMs, decision boundaries provide valuable insights into critical phenomena, including reasoning (Yang et al. 2025b), in-context learning (Zhao,

Nguyen, and Grover 2024), hallucination (Mayne et al. 2025), memorization (Li et al. 2025), and so on.

As a foundational concept in machine learning, the decision boundary represents a subspace of inputs where a model assigns equal probability to two distinct classification outcomes (Rosenblatt 1958). Extensive theoretical and empirical studies (Lee and Landgrebe 1997; Tumer and Ghosh 1996; Goodfellow, Shlens, and Szegedy 2015; Madry et al. 2018; Gu, Dolan-Gavitt, and Garg 2017) have demonstrated that the properties of decision boundaries reveal critical attributes of machine learning models, including performance, robustness, and generalization. Consequently, constructing and leveraging decision boundaries for LLMs becomes a powerful and promising approach to enhancing *almost all downstream analyses* of their behavior and capabilities.

Unfortunately, analyzing decision boundaries of LLMs incurs significantly greater complexity than for deep neural networks (DNNs) (Karimi, Derr, and Tang 2020; Karimi and Tang 2020; Li, Ding, and Gao 2019; Lee and Landgrebe 1997; Mickisch et al. 2020; Yousefzadeh and O’Leary 2019). Unlike classification tasks with a limited number of classes (Lee and Landgrebe 1997; Tumer and Ghosh 1996; Goodfellow, Shlens, and Szegedy 2015; Madry et al. 2018; Gu, Dolan-Gavitt, and Garg 2017), LLMs predict a single token from an expansive vocabulary, often exceeding 100,000 tokens. Moreover, their autoregressive nature (Bengio et al. 2003; Radford et al. 2018) requires iterative token predictions to generate complete sequences, which further compounds the complexity of modeling decision boundaries. For instance, a Qwen-3 model (with 8 billion parameters) (Yang et al. 2025a) supports sequences up to 32,768 tokens with a vocabulary of 151,936, resulting in approximately  $10^{169,790}$  decision regions! Such an enormous scale renders trivial attempts on decision-boundary-based analysis and visualization computationally infeasible. Prior studies (Zhao, Nguyen, and Grover 2024; Yang et al. 2025b; Mayne et al. 2025; Li et al. 2025), despite their valuable contributions to their specific motivating tasks, unfortunately sidestep this critical challenge. They either simplify the problem to toy scenarios, such as binary

\*Corresponding author.

classification (Zhao, Nguyen, and Grover 2024; Mayne et al. 2025), or use the decision boundary concept metaphorically without constructing it (Yang et al. 2025b; Li et al. 2025). Consequently, the haunting questions remain unanswered: **What constitutes an LLM’s decision boundary, and is there a universal yet efficient algorithm to construct it?**

To address these questions, we propose a principled strategy for modeling the decision boundaries of LLMs, which yields theoretical guarantees, computational tractability, and interpretability simultaneously. Inspired by the existing decision boundaries for multi-class classification, we treat generative language models as a composite multi-class classification task. As trivial solutions cannot model the complex decision boundaries for such tasks, we introduce a novel concept, namely *Decision Potential Surface (DPS)*, to facilitate decision boundary analysis. It is a landscape in which every point encodes the *competition potential* among candidate outputs, quantified by a *decision potential function (DPF)*. We theoretically demonstrate that the zero-height *isohypse* of the DPS corresponds to the decision boundary, with the enclosed regions representing decision regions.

By examining the definition of DPS, we surprisingly discover that enumerating the entire output space is unnecessary for computing the DPF. Instead, sufficient sampling already captures the “competition potential”. We therefore approximate the LLM’s decision boundary with only  $K$  finite ( $K \ll$  realistic classification count) sequence sampling, yielding  $K$ -DPS and keeping the theoretical error within a provably small bound. We establish the error bound, expected error bound, and error concentration between the ideal DPS and  $K$ -DPS, demonstrating that  $K$ -DPS offers a favorable trade-off between approximation accuracy and computational cost. Finally, we conduct extensive experiments on open-source LLMs to evaluate the empirical performance of our method.

To our best knowledge, this is the first study on constructing decision boundaries for LLMs. Moreover, our proposed *decision potential surface (DPS)* framework is the first to provide a practical approximation of decision boundaries with theoretical guarantees. Our contributions are as follows:

- We introduce the concepts of the *Decision Potential Function (DPF)* and *Decision Potential Surface (DPS)*. We prove that the *isohypses* of the decision potential surface represent the marginal decision boundaries of LLMs, with the zero-height isohypse equivalent to the decision boundary.
- We propose  $K$ -DPS, an efficient and bounded approximation of the ideal DPS that requires only finite sampling for each input. We theoretically and empirically establish the error bounds of this approximation relative to the ideal DPS and quantify the trade-off between approximation error and sampling size.
- Leveraging  $K$ -DPS, we present several insightful case studies that demonstrate how LLMs can be analyzed through the lens of their decision boundary properties.

## 2 Related Work

Decision-boundary analysis has long been used to understand model behavior, from linear classifiers (Rosenblatt

1958) to feedforward networks (Lee and Landgrebe 1997; Tumer and Ghosh 1996) and modern deep models. Prior work links boundary geometry to robustness, capacity, and failure modes: adversarial examples exploit locally linear boundaries (Goodfellow, Shlens, and Szegedy 2015), adversarial training smooths them (Madry et al. 2018), and backdoor attacks can be understood as hidden boundary shifts (Gu, Dolan-Gavitt, and Garg 2017). Subsequent studies further develop boundary extraction, visualization, and quantitative metrics for trained networks (Karimi, Derr, and Tang 2020; Karimi and Tang 2020; Lee and Landgrebe 1997; Mickisch et al. 2020; Yousefzadeh and O’Leary 2019). For LLMs, boundary-oriented analysis remains less developed. Existing studies investigate decision behavior in restricted settings, including in-context learning (Zhao, Nguyen, and Grover 2024), confidence and counterfactual reliability (Mayne et al. 2025), and boundary-aware reasoning (Yang et al. 2025b). However, they do not provide a general construction of decision boundaries for autoregressive sequence generation, nor a finite-sampling error theory for such construction. Our work addresses this gap by defining DPS for LLM sequence decisions and deriving a practical  $K$ -sample approximation with explicit error guarantees. A more detailed related work discussion is provided in Appendix B.

## 3 Decision Boundary of Language Models

### 3.1 Decision Boundary on Classification Models

We begin our theoretical analysis with traditional classification models and aim to extend the insights to generative language models.

Consider a neural network  $f : \mathbb{R}^d \rightarrow \mathbb{R}^M$  that maps an input sample  $\mathbf{x} \in \mathbb{R}^d$  to a predicted probability distribution over  $M$  classes, where the set of classes can be denoted as  $\mathcal{M} = \{1, 2, \dots, M\}$ , with  $M > 2$ . Our goal is to characterize the decision boundary of  $f$  under a specific input data distribution  $\mathcal{D} \subseteq \mathbb{R}^d$ . Without loss of generality, we decompose  $f$  into three components: (i) A representation module  $h = f_r(\mathbf{x}) : \mathbb{R}^d \rightarrow \mathbb{R}^{d'}$  that maps the input  $\mathbf{x}$  to a latent representation  $h$ . (ii) A linear classification head  $z = f_{\text{cls}}(h) = W_{\text{cls}}h + b_{\text{cls}} : \mathbb{R}^{d'} \rightarrow \mathbb{R}^M$ , where  $W_{\text{cls}} \in \mathbb{R}^{M \times d'}$  and  $b_{\text{cls}} \in \mathbb{R}^M$  are learnable parameters, projecting the representation  $h$  into classification logits  $z$ . (iii) A nonlinear normalization function  $P = \sigma(z) : \mathbb{R}^M \rightarrow \mathbb{R}^M$ , which transforms the logits into a probability distribution  $P = [p_1, p_2, \dots, p_M]$ , where  $0 \leq p_i \leq 1$  for  $i = 1, \dots, M$  and  $\sum_{i=1}^M p_i = 1$ . The final predicted class for  $\mathbf{x}$  can be determined by  $\arg \max_i p_i$ . Then, the decision boundary of the neural network  $f$  is defined as follows.

**Definition 3.1** (Decision Boundary of  $f$ ). The decision boundary of a neural network  $f$  under an input distribution  $\mathbf{x} \in \mathcal{D}$  is the set of inputs for which at least two classes in  $\mathcal{M} = \{1, 2, \dots, M\}$  have equal and maximal prediction probabilities. Formally, we denote this set as  $\mathcal{B}_M^{(f, \mathcal{D})}$ , defined by:

$$\mathcal{B}_M^{(f, \mathcal{D})} = \{\mathbf{x} \in \mathcal{D} \mid \exists m, n \in \mathcal{M}, m \neq n, \text{ such that } p_m = p_n \text{ and } p_m \geq \max_{o \in \mathcal{M} \setminus \{m, n\}} p_o\}, \quad (1)$$

where  $p_i = P[i] = \sigma(f_{\text{cls}}(f_r(\mathbf{x}))) [i]$  is the predicted probability for class  $i$ .

Based on Definition 3.1, we characterize the decision boundary for multi-class classification scenarios as follows.

**Theorem 3.2** (Properties of Multi-Class Classification Boundary). *For multi-class classification ( $M > 2$ ), the decision boundary of  $f$  can be expressed as:*

$$\begin{aligned} \mathcal{B}_M^{(f, \mathcal{D})} &= \bigcup_{1 \leq m < n \leq M} \mathcal{B}_{mn}, \\ \mathcal{B}_{mn} &= \{\mathbf{x} \mid (w_m - w_n)h + (b_m - b_n) = 0, \\ & z_m = z_n \geq z_o \forall o \neq m, n, h = f_r(\mathbf{x}), \mathbf{x} \in \mathcal{D}\}. \end{aligned} \quad (2)$$

where  $z = W_{\text{cls}}h + b_{\text{cls}}$  is the logits,  $w_m$  and  $w_n$  are the  $m$ -th and  $n$ -th rows of  $W_{\text{cls}}$ , and  $b_m, b_n$  are the corresponding entries of  $b_{\text{cls}}$ .

Geometrically,  $\mathcal{B}_M$  induces a Voronoi partition of the representation space, where each class (i.e., decision regions) corresponds to a Voronoi cell.

The proof of Theorem 3.2 is provided in Appendix C.1.

### 3.2 Decision Boundary for Language Models

An LLM  $f : \mathcal{V}^{N_q} \rightarrow \mathcal{V}^{N_r}$  generates a sequence of tokens  $\mathbf{y} = [y_1, \dots, y_{N_r}]$ , where each token  $y_t \in \mathcal{V} = \{1, 2, \dots, V\}$  is drawn from a vocabulary of size  $V$ , conditioned on an input prompt  $\mathbf{x} = [x_1, \dots, x_{N_q}] \in \mathcal{V}^{N_q}$ .  $N_q$  and  $N_r$  are the sequence lengths of the input and generated texts. At each generation step  $t$ , the LLM predicts the next token  $y_t$  based on the prompt and previously generated tokens, i.e.,  $y_t \sim P_f(y_t | \mathbf{x}, y_1, \dots, y_{t-1})$ . This single-step generation can be viewed as a multi-class classification over  $\mathcal{V}$ , and thus, the single-token decision boundary follows Theorem 3.2. When defining the decision boundary for the entire sequence  $\mathbf{y} \in \mathcal{V}^{N_r}$ , we first model the joint probability of the sequence under the autoregressive process. We derive the decision boundary of LLMs from that of multi-classification, as shown below.

**Theorem 3.3** (Decision Boundary of Language Models). *The decision boundary of an LLM  $f$  under an input text distribution  $\mathcal{D}' \subseteq \bigcup_{n_q=1}^{N_q} \mathcal{V}^{n_q}$  is the set of prompts  $\mathbf{x} \in \mathcal{D}'$  that lead to **equal generation probabilities** for at least two distinct sequences  $\mathbf{y}_v, \mathbf{y}_w \in \mathcal{V}^{N_r}$ , with their probabilities being maximal. Formally, the decision boundary  $\mathcal{B}_{\text{llm}}^{(f, \mathcal{D}')}$  is:*

$$\begin{aligned} \mathcal{B}_{\text{llm}}^{(f, \mathcal{D}')} &= \bigcup_{\mathbf{y}_v \neq \mathbf{y}_w \in \mathcal{V}^{N_r}} \mathcal{B}_{\text{llm}, \mathbf{y}_v, \mathbf{y}_w}, \quad \mathcal{B}_{\text{llm}, \mathbf{y}_v, \mathbf{y}_w} = \{\mathbf{x} \in \mathcal{D}' \mid \\ & P_f(\mathbf{y}_v | \mathbf{x}) = P_f(\mathbf{y}_w | \mathbf{x}) \geq \max_{\mathbf{y}_u \in \mathcal{V}^{N_r} \setminus \{\mathbf{y}_v, \mathbf{y}_w\}} P_f(\mathbf{y}_u | \mathbf{x})\}, \end{aligned} \quad (3)$$

where  $P_f(\mathbf{y} | \mathbf{x}) = \prod_{t=1}^{N_r} P_f(y_t | \mathbf{x}, y_1, \dots, y_{t-1})$  is the joint probability of generating sequence  $\mathbf{y}$  given prompt  $\mathbf{x}$ .

The proof of Theorem 3.3 is provided in Appendix C.2.

While Theorem 3.3 provides a concise and intuitive definition of decision boundary for LLMs, analyzing or computing this boundary could be computationally impossible in practice. As analyzed in Section 1, the primary challenge stems from the large vocabulary size and the autoregressive nature

of sequence generation, i.e., for a generation of length  $N_r$ , the total number of possible sequences is  $V^{N_r}$ , leading to an *exponential growth* of decision regions. Specifically, the decision boundary defined in Equation (3) involves comparing  $\mathbf{y}_v, \mathbf{y}_w \in \mathcal{V}^{N_r}$ , resulting in up to  $\binom{V^{N_r}}{2} \approx \frac{(V^{N_r})^2}{2}$  pairwise comparisons. This is neither computationally feasible nor interpretable in subsequent visualizations.

Given the intractability of directly analyzing the decision boundary defined in Theorem 3.3, a new strategy for constructing the decision boundary of large language models is essential. Specifically, this new construction should satisfy the following criteria: First, it must be **theoretically rigorous**, meaning the construction should be equivalent to or provide a bounded approximation of the decision boundary defined in Theorem 3.3, ensuring consistency with the formal definition of the boundary separating prompts that yield different output sequences. Second, the method should be **practical**, meaning it must be computationally efficient and feasible for implementation, enabling the modeling of decision boundaries for industrial-scale LLMs with large vocabularies and long generation lengths. Third, the method should be **interpretable**, meaning the constructed decision boundary should explicitly capture key properties of LLMs (e.g., curvature), and provide interpretable insights into phenomena observed in LLM behavior, such as output variability or robustness.

In the next section, we will introduce an approximation procedure for the decision boundary defined in Theorem 3.3, addressing these criteria to enable practical and meaningful analysis of LLMs.

## 4 K-Grained Decision Potential Surface

In this section, we introduce the *Decision Potential Surface* (DPS), a novel concept for analyzing the decision boundaries of LLMs by representing the *decision potential* of generated sequences as a surface over the input manifold. In Section 4.1, we formally define DPS and establish its relationship with the standard decision boundary formulation in LLMs. In Section 4.2, we propose  $K$ -grained DPS ( $K$ -DPS), a practical approximation of DPS, and theoretically derive its error bounds with respect to the ideal DPS.

### 4.1 Decision Potential Surface of LLMs

**Definition 4.1** (Decision Potential Surface of Language Models). Given an input text distribution  $\mathbf{x} \in \mathcal{D}'$  with  $\mathcal{D}' \subseteq \bigcup_{n_q=1}^{N_q} \mathcal{V}^{n_q}$  and a language model  $f : \mathcal{V}^{N_q} \rightarrow \mathcal{V}^{N_r}$  that generates an output sequence  $\mathbf{y} = f(\mathbf{x}) = \arg \max_{\mathbf{y}_s \in \mathcal{V}^{N_r}} P_f(\mathbf{y}_s | \mathbf{x})$ , we define the *decision potential function* (DPF)  $\Phi_f^\infty(\mathbf{x}) : \mathcal{D}' \rightarrow \mathbb{R}_+$  as the squared difference in log-likelihoods between the top two generated sequences under the input prompt  $\mathbf{x}$ , i.e.,

$$\begin{aligned} \Phi_f^\infty(\mathbf{x}) &= \left( \min_{\mathbf{y}_w \in \mathcal{V}^{N_r}, \mathbf{y}_v \neq \mathbf{y}_w} \left[ \max_{\mathbf{y}_v \in \mathcal{V}^{N_r}} \log P_f(\mathbf{y}_v | \mathbf{x}) - \log P_f(\mathbf{y}_w | \mathbf{x}) \right] \right)^2 \\ &= (\log P_f(\mathbf{y}_{1*} | \mathbf{x}) - \log P_f(\mathbf{y}_{2*} | \mathbf{x}))^2, \end{aligned} \quad (4)$$

where  $\mathbf{y}_{1*}, \mathbf{y}_{2*} \in \mathcal{V}^{N_r}$  denote the sequences with the highest and second-highest log-likelihoods, respectively. The *decision potential surface (DPS)* is then defined as  $\mathcal{S}^{(f, \mathcal{D}')} := \{\Phi_f^\infty(\mathbf{x}) \mid \mathbf{x} \in \mathcal{D}'\}$ .

Intuitively,  $\mathcal{S}^{(f, \mathcal{D}')}$  can be viewed as a surface representing the competitive likelihoods across all inputs, where each decision potential value  $\Phi_f^\infty(\mathbf{x})$  quantifies the *confidence* in distinguishing the most likely sequence.

**Remark 4.2** (The Top-1/Top-2 Construction Is Naturally Multiclass, Not Binary). *The use of only the top two sequences in Definition 4.1 follows the classical definition of multiclass decision boundaries. A multiclass boundary is not obtained by comparing all classes simultaneously at every input point; rather, as established in Theorem 3.2, it is the union of local pairwise boundaries where the two maximal classes tie. In the LLM setting, the “classes” are possible generated sequences or token continuations. Therefore, restricting attention to the top-1 and top-2 sequences is not a binary approximation but the standard local characterization of a multiclass decision boundary.*

Following Definition 4.1, we define *isohypses* (i.e., contour lines) on the surface  $\mathcal{S}^{(f, \mathcal{D}')}$  as follows:

**Definition 4.3** ( $\varepsilon$ -Isohypse). The  $\varepsilon$ -isohypse on the decision potential surface  $\mathcal{S}^{(f, \mathcal{D}')}$  is the set of inputs with the same decision potential value  $\varepsilon$ , i.e.,

$$\mathcal{D}'_{(\varepsilon, f)} = \{\mathbf{x} \mid \mathbf{x} \in \mathcal{D}'; \Phi_f^\infty(\mathbf{x}) = \varepsilon\}. \quad (5)$$

As a degenerate case, the zero level set of  $\mathcal{S}^{(f, \mathcal{D}')}$  exhibits the following property:

**Theorem 4.4** (0-Isohypse as the Decision Boundary). *The decision boundary of a language model  $f(\mathbf{x})$  under  $\mathcal{D}'$ , as defined in Theorem 3.3, is equivalent to the 0-isohypse, i.e.,*

$$\mathcal{B}_{llm}^{(f, \mathcal{D}')} = \mathcal{D}'_{(0, f)} = \{\mathbf{x} \in \mathcal{D}' \mid \Phi_f^\infty(\mathbf{x}) = 0\}, \quad (6)$$

where regions separated by the 0-isohypse correspond exactly to the Voronoi cells.

We also provide the following corollary to characterize the surface structure:

**Corollary 4.5** ( $\varepsilon$ -Isohypse Gives  $\sqrt{\varepsilon}$ -nat Confidence Hierarchy). *For any  $\varepsilon > 0$ , the input space  $\mathcal{D}'$  is partitioned into three disjoint strata:*

- $\varepsilon$ -barrier:  $\mathcal{D}'_{(>\varepsilon, f)} = \{\mathbf{x} \mid \Phi_f^\infty(\mathbf{x}) > \varepsilon; \mathbf{x} \in \mathcal{D}'\}$ , where  $f(\mathbf{x})$  predicts the sequence of its region with at least  $\sqrt{\varepsilon}$  nats (natural units of information) of confidence over the next most likely sequence.
- $\varepsilon$ -well:  $\mathcal{D}'_{(<\varepsilon, f)} = \{\mathbf{x} \mid \Phi_f^\infty(\mathbf{x}) < \varepsilon; \mathbf{x} \in \mathcal{D}'\}$ , where  $f(\mathbf{x})$  has low confidence, with a margin less than  $\sqrt{\varepsilon}$  nats. As  $\varepsilon \rightarrow 0$ , this stratum converges to the 0-isohypse.
- $\varepsilon$ -isohypse:  $\mathcal{D}'_{(\varepsilon, f)} = \{\mathbf{x} \in \mathcal{D}' \mid \Phi_f^\infty(\mathbf{x}) = \varepsilon\}$ , representing the contour where the confidence margin is exactly  $\sqrt{\varepsilon}$  nats.

Proofs are provided in Appendix C.3 and C.4, respectively. Given Theorem 4.4, we can construct the DPS defined in Definition 4.1 to characterize the decision boundaries of

LLMs. Unfortunately, computing the decision boundary or visualizing the DPS based on Definition 4.1 remains computationally infeasible, as evaluating  $\Phi_f^\infty(\mathbf{x})$  in Equation (4) requires considering all possible sequences in  $\mathcal{V}^{N_r}$ , resulting in a computational complexity the same as before.

Fortunately, as Equation (4) depends only on the log-likelihoods of the top two sequences, we can propose an efficient approximation with a modest error, detailed in the next subsection.

## 4.2 K-Grained Decision Potential Surface

We introduce  $K$ -grained decision potential surface for approximating  $\mathcal{S}^{(f, \mathcal{D}')}$ :

**Definition 4.6** ( $K$ -Grained Decision Potential Surface). Given  $\mathbf{x} \in \mathcal{D}'$  and a language model  $f(\mathbf{x})$ , we define the  $K$ -grained potential function  $\Phi_f^K(\mathbf{x}) : \mathcal{D}' \rightarrow \mathbb{R}_+$  as

$$\begin{aligned} \Phi_f^K(\mathbf{x}) &= \left( \min_{\mathbf{y}_w \in \mathcal{Y}_K, \mathbf{y}_w \neq \mathbf{y}_v} \left[ \max_{\mathbf{y}_v \in \mathcal{Y}_K} \log P_f(\mathbf{y}_v | \mathbf{x}) - \log P_f(\mathbf{y}_w | \mathbf{x}) \right] \right)^2 \\ &= (\log P_f(\mathbf{y}_{1*}^K | \mathbf{x}) - \log P_f(\mathbf{y}_{2*}^K | \mathbf{x}))^2, \end{aligned} \quad (7)$$

where  $1 \ll K \ll V^{N_r}$  denotes the size of output space for each input,  $\mathcal{Y}_K = \{\mathbf{y}_v \sim P_f(\cdot | \mathbf{x}) \mid v = 1, \dots, K\}$  denotes  $K$  i.i.d. (independent and identically distributed) sampled texts, and  $\mathbf{y}_{1*}^K$  and  $\mathbf{y}_{2*}^K$  denote the top two generated texts with the largest generation log-likelihoods within  $\mathcal{Y}_K$ .

In this way, the computational complexity of constructing the decision boundary is reduced from  $\mathcal{O}(V^{2N_r} \cdot |\mathcal{D}'|)$  to  $\mathcal{O}(K^2 \cdot |\mathcal{D}'|)$ , resulting in a substantial reduction. This naturally leads to the next question: what is the error between  $\Phi_f^K(\mathbf{x})$  and  $\Phi_f^\infty(\mathbf{x})$ ? We address this by theoretically analyzing their relationship in the following theorems.

**Theorem 4.7** (Error Bound for Estimating  $\Phi_f^\infty(\mathbf{x})$  with  $\Phi_f^K(\mathbf{x})$ ). *For a fixed input  $\mathbf{x} \in \mathcal{D}'$  and a set  $\mathcal{Y}_K$  of  $K$  i.i.d. samples drawn from the language model’s output distribution  $P_f(\cdot | \mathbf{x})$ , suppose the population top-2 gap satisfies  $\Delta_\infty(\mathbf{x}) = \log P_f(\mathbf{y}_{1*} | \mathbf{x}) - \log P_f(\mathbf{y}_{2*} | \mathbf{x}) \leq R_K(\mathbf{x})$ , where  $R_K(\mathbf{x}) = \log P_f(\mathbf{y}_{1*}^K | \mathbf{x}) - \min_{\mathbf{y} \in \mathcal{Y}_K} \log P_f(\mathbf{y} | \mathbf{x})$  represents the log-likelihood diameter of  $\mathcal{Y}_K$ . Then, for any  $\delta \in (0, 1)$ , the error between the sample-based decision potential  $\Phi_f^K(\mathbf{x})$  and the true decision potential  $\Phi_f^\infty(\mathbf{x})$  satisfies:*

$$|\Phi_f^K(\mathbf{x}) - \Phi_f^\infty(\mathbf{x})| \leq 2R_K^2(\mathbf{x}) \sqrt{\frac{\log(4/\delta)}{2K}}, \quad (8)$$

with probability at least  $1 - \delta - 2\varepsilon_{tail}$ , where  $\varepsilon_{tail} = (1 - P_f(\mathbf{y}_{1*}^K | \mathbf{x}))^K$ .

**Theorem 4.8** (Local Candidate-Set Bound). *For a fixed input  $\mathbf{x} \in \mathcal{D}'$ , let  $\Delta_\infty(\mathbf{x}) = \log P_f(\mathbf{y}_{1*} | \mathbf{x}) - \log P_f(\mathbf{y}_{2*} | \mathbf{x})$ . For any  $\eta \geq 0$ , define the local near-second candidate set*

$$\mathcal{Y}_{2, \eta}(\mathbf{x}) = \{\mathbf{y} \in \mathcal{V}^{N_r} : \mathbf{y} \neq \mathbf{y}_{1*}, \log P_f(\mathbf{y} | \mathbf{x}) \geq \log P_f(\mathbf{y}_{2*} | \mathbf{x}) - \eta\}. \quad (9)$$

Let

$$p_{2,\eta}(\mathbf{x}) = \sum_{\mathbf{y} \in \mathcal{Y}_{2,\eta}(\mathbf{x})} P_f(\mathbf{y}|\mathbf{x}) \quad (10)$$

be the probability mass of this local candidate set. Then

$$|\Phi_f^K(\mathbf{x}) - \Phi_f^\infty(\mathbf{x})| \leq \eta(2\Delta_\infty(\mathbf{x}) + \eta) \quad (11)$$

with probability at least

$$1 - (1 - P_f(\mathbf{y}_{1*}|\mathbf{x}))^K - (1 - p_{2,\eta}(\mathbf{x}))^K. \quad (12)$$

Equivalently, when  $p_{2,\eta}(\mathbf{x}) > 0$ , if

$$K \geq \max \left\{ \frac{\log(2/\delta)}{P_f(\mathbf{y}_{1*}|\mathbf{x})}, \frac{\log(2/\delta)}{p_{2,\eta}(\mathbf{x})} \right\}, \quad (13)$$

then Equation (11) holds with probability at least  $1 - \delta$ .

**Theorem 4.9** (Expected Error Bound). *Under the same conditions as Theorem 4.7, the expected error between the sample-based decision potential  $\Phi_f^K(\mathbf{x})$  and the true decision potential  $\Phi_f^\infty(\mathbf{x})$  is bounded as:*

$$\mathbb{E} [|\Phi_f^K(\mathbf{x}) - \Phi_f^\infty(\mathbf{x})|] \leq 2R_K^2(\mathbf{x}) \sqrt{\frac{2\pi}{K}} + 4R_K^2(\mathbf{x})\varepsilon_{tail}, \quad (14)$$

where  $\varepsilon_{tail} = (1 - P_f(\mathbf{y}_{1*}^K|\mathbf{x}))^K$ .

**Corollary 4.10** (Concentration Bound). *Under the same conditions as Theorem 4.7, for any  $\lambda > 0$ , the tail probability of the error satisfies:*

$$\Pr \left( |\Phi_f^K(\mathbf{x}) - \Phi_f^\infty(\mathbf{x})| \geq \lambda \right) \leq 4 \exp \left( -\frac{K\lambda^2}{2R_K^4(\mathbf{x})} \right) + 2\varepsilon_{tail}, \quad (15)$$

where  $\varepsilon_{tail} = (1 - P_f(\mathbf{y}_{1*}^K|\mathbf{x}))^K$ .

Proofs are provided in Appendix C.5, Appendix C.6, Appendix C.7, and Appendix C.8, respectively.

The estimation error contracts with  $K$  at the familiar  $1/\sqrt{K}$  rate, mirroring the decay of an empirical mean. The tail probability  $\varepsilon_{tail}$  bounds the chance that the true top-1 candidate is absent from  $\mathcal{Y}_K$ . This term depends on the concentration of the output distribution and is exponentially suppressed as  $K$  grows. In practice, its magnitude differs across generation regimes: *i) Ordinary generation.* When  $N_r$  is small, the top sequences carry substantial joint probability mass, and  $\varepsilon_{tail}$  becomes negligible at modest  $K$  (e.g.,  $K \approx 10^3$ ). Token-level DPS ( $N_r = 1$ , Section 4.3) is even more favorable, as the output space is only the vocabulary. *ii) Long or high-entropy generation.* Very long, high-entropy generation can produce tiny joint probabilities for any individual sequence. This is an inherent difficulty of sequence-level decision-boundary construction for LLMs, not a defect specific to DPS. In such regimes, one may instead rely on prefix-conditioned token-level DPS or report empirical stability curves (Section 5.4) rather than relying merely on the joint-probability tail term.

The common factor  $R_K(\mathbf{x})$  is a worst-case log-likelihood diameter dictated by the least likely sentence that happens to be sampled. Theorem 4.8 gives a sharper local alternative: the error depends on the tolerance  $\eta$  around the true second-best

candidate and on the probability mass  $p_{2,\eta}(\mathbf{x})$  of candidates in that local band. When  $\eta = 0$ , the bound becomes exact: if the sample contains the true top-1 sequence and any true second-best sequence, then  $\Phi_f^K(\mathbf{x}) = \Phi_f^\infty(\mathbf{x})$ . For larger  $\eta$ , the theorem separates candidate discovery ( $P_f(\mathbf{y}_{1*}|\mathbf{x})$  and  $p_{2,\eta}(\mathbf{x})$ ) from gap distortion ( $\eta(2\Delta_\infty + \eta)$ ), avoiding dependence on the least likely sampled sentence.

### 4.3 Variants of $K$ -DPS

**Semantically Similar Text Completions.** One may ask whether the top-1 and top-2 completions are often nearly identical, which could inflate DPS values artificially and obscure genuine decision boundaries. DPS naturally accommodates this scenario. On the one hand, DPS is defined on the raw sequence/token probability space of the language model, where semantic similarity between completions is not ignored but naturally reflected in the geometry. On the other hand, semantically equivalent outputs occupy adjacent or overlapping decision regions, producing narrow basins that match the intuition of a smooth semantic equivalence class, and this clustering is an emergent feature of the multiclass decision boundary. An empirical validation of this point is provided in Appendix (Table 1). We further discuss how to filter similar texts when desired and why such filtering does not make the theoretical guarantees depend on the worst-case diameter  $R_K(\mathbf{x})$  in Appendix D.2.

**Influence of Sampling Strategies.** Sampling temperature and other decoding strategies change the output distribution and thus the numerical values of the DPS, without invalidating the framework. The DPS is defined on the model’s raw output distribution (Definition 4.1), raising a natural question: is it compatible with different decoding strategies?

The answer is affirmative, though the nature of compatibility varies by strategy. As proved in Appendix D.4, temperature scaling constitutes a monotone transformation of the DPS: for any temperatures  $T_1 < T_2$ , the ordering of output sequences by log-probability is preserved, so the zero-height isohypse  $\mathcal{D}'_{(0,f)}$  and the decision boundary structure remain identical. Higher temperature compresses the surface vertically by a factor of  $1/T^2$ , reducing the dynamic range of DPS values, while lower temperature amplifies local contrast. All topological features, including the arrangement of isohypses, are strictly preserved.

Other decoding strategies require separate treatment, as discussed in Appendix D.5. Nucleus (top- $p$ ) sampling restricts candidates to a high-probability subset of the model’s support, leaving the error bounds of Theorems 4.7–4.10 valid with slightly adjusted tail constants for typical  $p \in [0.9, 1.0)$ . Top- $k$  sampling, when  $k$  is small, alters the sampling distribution more substantially and requires modified theoretical bounds; we recommend  $k \geq 50$  so that the top tokens at each step are reliably included, which suffices for accurate DPS estimation at modest  $K$ .

**Token-Level DPS.** While the preceding sections focus on sequence-level decision boundary construction, a degenerate case, namely token-level DPS, merits separate discussion. The sequence-level definition in Equation (4) naturally supports token-level analysis as the special case  $N_r = 1$ .

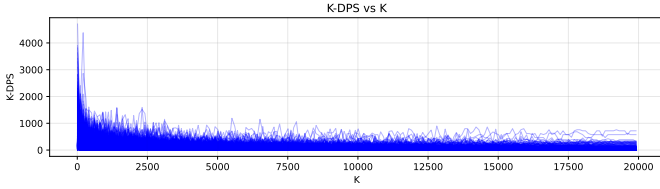


Figure 1: Effect of sampling size  $K$  on the  $K$ -DPS value.

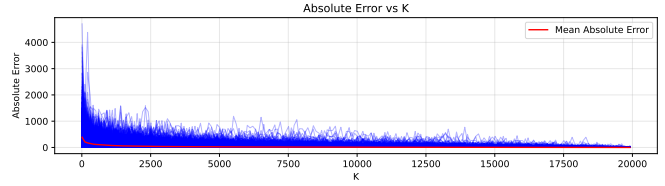


Figure 2: Absolute error between the high-budget reference  $K$ -DPS ( $K = 20,000$ ) and estimates with varying  $K$ .

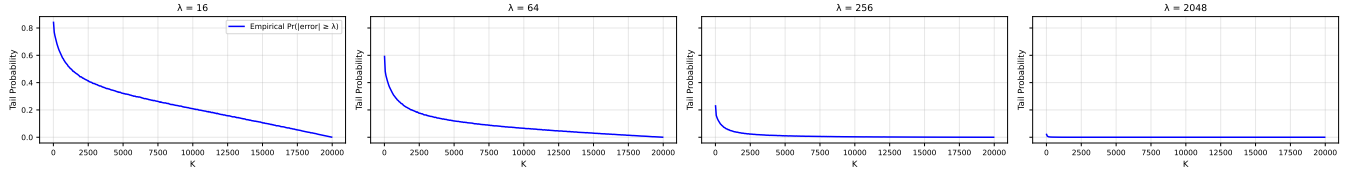


Figure 3: Empirical concentration experiments with different  $\lambda$  values.

For a generation step  $t$ , the input consists of the prompt concatenated with the previously generated prefix  $\mathbf{x}' = [\mathbf{x}, y_1, \dots, y_{t-1}]$ , and the output classes are the vocabulary tokens  $\mathcal{V}$ . The decision potential function reduces to the squared log-likelihood difference between the top two tokens, while all theoretical guarantees (Theorems 4.7–4.10) carry over with the output space being only  $V$  categories.

## 5 Empirical Analysis

### 5.1 Settings

**Datasets and Models.** We utilize both pre-training corpora and supervised fine-tuning (SFT) datasets to simulate the input data distribution for constructing decision boundaries and the decision potential surface. For the pre-training corpus, we select Wikipedia Mini (Ridder and Schilling 2025), an unsupervised text corpus containing a condensed version of Wikipedia articles. For supervised fine-tuning, we employ Tulu-3-SFT-MIX (Lambert et al. 2025), OpenO1-SFT (Xia et al. 2025a), HH-RLHF (Ganguli et al. 2022), and Alpaca (Taori et al. 2023), all of which are widely used in academic and industrial settings. We use Llama3.2-1B (Grattafiori et al. 2024) as the basic backbone, and employ Llama-3.1 (8B) (Grattafiori et al. 2024), Llama-Guard-3 (8B) (Grattafiori et al. 2024), Mistral (7B) (Jiang et al. 2023), Zephyr (7B) (Tunstall et al. 2023), and Tulu-2 (7B) (Iverson et al. 2023) for the alignment decision boundary analysis, and utilize the Llama-2 (7B) (Touvron et al. 2023) for the machine unlearning experiments.

**Implementation Details.** For sampling, we use *nucleus sampling* in our  $K$ -DPS implementation, with the clipping probability  $p$  set to 0.9. In subsequent experiments, each data point is repeated five times. The experiments are conducted on  $4 \times 94\text{GB}$  Nvidia Tesla H100 NVL GPUs.

### 5.2 Influence of Sampling Grain $K$

We first evaluate the impact of the key hyperparameter, the sampling grain  $K$ , on the  $K$ -DPS value and the absolute errors between  $K$ -DPS and the ideal DPS. Specifically, we

set  $K = 20,000$  as a high-budget reference estimator to approximate the ideal DPS (exact exhaustive enumeration of  $\mathcal{V}^{N_r}$  being computationally infeasible for modern LLMs). We then compute the  $K$ -DPS values by varying  $K$  from 10 to 20,000 to illustrate how the decision potential value  $\Phi_f^K(\cdot)$  converges to the reference  $\Phi_f^{20,000}(\cdot)$ . Similarly, we calculate the absolute errors of  $\Phi_f^K(\cdot)$  across different settings of  $K$ . As shown in Figure 1, the potential values rapidly converge to the reference values (represented by horizontal lines at the tails), indicating that a relatively small  $K$  can yield a highly accurate decision potential surface. Moreover, by examining the errors defined in Equation (8), as depicted in Figure 2, we observe that both the absolute error for individual samples and the empirical average error decrease to zero, confirming the effectiveness of  $K$ -DPS. Figures 1 and 2 also serve as valuable references for selecting appropriate  $K$  values. More error analysis can be found in the Appendix.

### 5.3 Empirical Concentration Bias

We also present an empirical study of concentration experiments, focusing on the trend of sample probabilities for inputs with a decision potential error exceeding a given fixed value  $\lambda$  across various sampling sizes  $K$ . As shown in Figure 3, we evaluate the tail probability for  $K$  values ranging from 10 to 20,000, with  $\lambda$  set to 16, 64, 256, and 2048. These  $\lambda$  values represent the geometric errors between the approximate and ideal DPS values. It is noteworthy to emphasize that even a  $\lambda$  value of 256 is not excessively large or insignificant, as our decision potential function  $\Phi_f^K(\cdot)$  is defined as the **square** of logarithmic errors, as specified in Equation 7.

From Figure 3, we observe that the tail probabilities exhibit an exponential decrease, indicating that the likelihood of exceeding a given error bound diminishes significantly with a linear increase in the sampling size  $K$ . Specifically, Figure 3 demonstrates that a sampling size of 10,000 ensures an absolute error below 64 with 90% confidence and an error below 256 with 99% probability. These results align closely with our absolute error analysis presented in Figure 2.

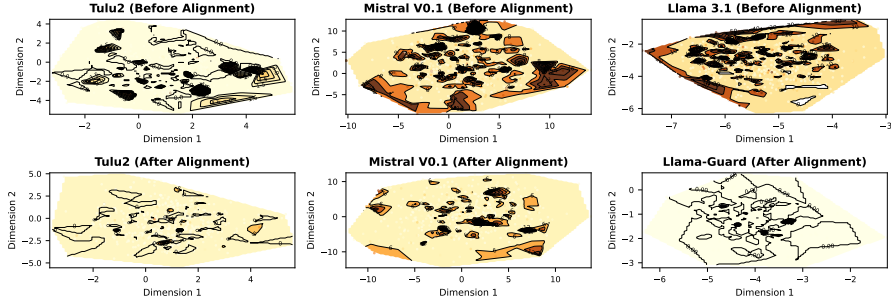


Figure 4: Comparison of  $K$ -DPS for models before and after alignment. A deeper color indicates a higher  $K$ -DPS score.

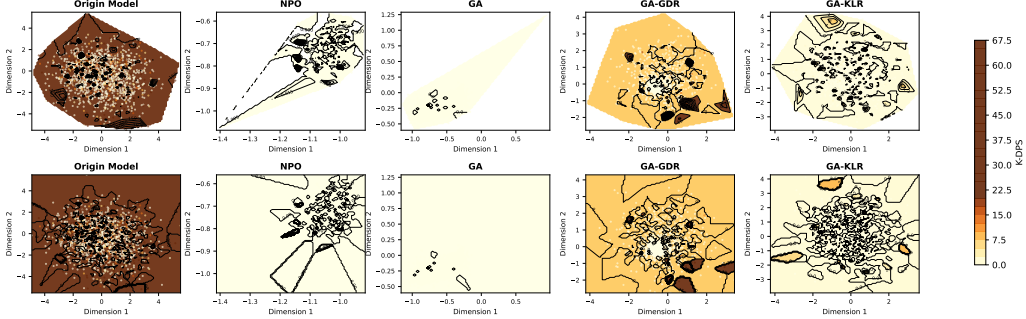


Figure 5: Comparison of  $K$ -DPS among different machine unlearning algorithms. The first and second rows indicate the visualization under linear and nearest interpolation, respectively.

## 5.4 Implications

In this section, we choose two critical topics on LLMs, alignment and machine unlearning, as proof-of-concept examples to demonstrate the effectiveness of  $K$ -DPS for intuitively interpreting LLMs.

**Alignment.** We use  $K = 2,500$  for the alignment experiments, with input queries from AdvBench (Zou et al. 2023). As shown in Figure 4, the decision boundary of aligned models becomes dramatically smoother and flatter compared to their pre-alignment counterparts when evaluated on adversarial prompts from AdvBench. This indicates that alignment substantially reduces regions of high confidence in harmful outputs and creates broad, low- $K$ -DPS basins that strongly favor refusal. This geometric transformation directly explains both: *i) Why jailbreaks succeed on unaligned models*: they target narrow, high-confidence “vulnerability spikes” that remain in the pre-alignment landscape; *ii) Why alignment mitigates most jailbreaks*: it eliminates these spikes entirely, making harmful responses probabilistically unlikely across vast regions of prompt space. Note that this phenomenon is observed from the height of the surface, which is not affected by dimensionality reduction.

**Machine Unlearning.** We apply our  $K$ -DPS to two representative unlearning methods: Gradient Ascent (GA) (Yao et al. 2024) and Negative Preference Optimization (NPO) (Zhang et al. 2024). We use the standard Harry Potter book as the forget (unlearning) corpus and a Wikipedia subset (Ridder and Schilling 2025) as the retain set. During unlearning, we continue training on the retain set using standard gradient

descent (GDR) or the KL divergence (KLR) from the original model. We set  $K = 2,000$ . As shown in Figure 5, our  $K$ -DPS visualizations provide a far clearer picture of the side effects of unlearning than previously possible (Liu et al. 2025a; Geng et al. 2025). While current works could merely report that unlearning without proper retention training degrades overall performance, they are unable to show what form this degradation takes in the model’s internal decision process. With  $K$ -DPS, we reveal that naïve unlearning methods (e.g., GA) can trigger catastrophic collapse of the entire decision manifold, where large portions of the prompt space that were previously smooth become extremely jagged and fragmented, with erratic high- and low- $K$ -DPS spikes appearing in regions unrelated to the forget corpus. In contrast, when retention training is included, the damage is substantially mitigated. The above observations demonstrate that  $K$ -DPS not only confirms known phenomena at a qualitative level but, for the first time, makes the geometric nature of “machine unlearning damage” directly observable and comparable across different methods.

## 6 Conclusion

We propose DPS, a decision-boundary formulation for LLM sequence generation, and  $K$ -DPS, a finite-sampling approximation that makes boundary construction computationally feasible. We prove that the zero-height isohypse of DPS recovers the decision boundary and derive absolute, expected, concentration, and local candidate-set error bounds. Experiments further show that  $K$ -DPS converges with practical

sampling budgets and reveals interpretable boundary changes under alignment and unlearning.

## References

- Allen-Zhu, Z.; and Li, Y. 2025. Physics of Language Models: Part 3.2, Knowledge Manipulation. In *13th International Conference on Learning Representations, ICLR 2025*.
- Ameisen, E.; Lindsey, J.; Pearce, A.; Gurnee, W.; Turner, N. L.; Chen, B.; Citro, C.; Abrahams, D.; Carter, S.; Hosmer, B.; et al. 2025. Circuit tracing: Revealing computational graphs in language models. *Transformer Circuits Thread*, 6.
- Bengio, Y.; Ducharme, R.; Vincent, P.; and Jauvin, C. 2003. A Neural Probabilistic Language Model. *J. Mach. Learn. Res.*, 3: 1137–1155.
- Biderman, S.; Schoelkopf, H.; Anthony, Q. G.; et al. 2023. Pythia: A Suite for Analyzing Large Language Models Across Training and Scaling. In Krause, A.; Brunskill, E.; Cho, K.; Engelhardt, B.; Sabato, S.; and Scarlett, J., eds., *International Conference on Machine Learning, ICML 2023, 23-29 July 2023, Honolulu, Hawaii, USA*, Proceedings of Machine Learning Research, 2397–2430. PMLR.
- Conmy, A.; Mavor-Parker, A. N.; Lynch, A.; Heimersheim, S.; and Garriga-Alonso, A. 2023. Towards Automated Circuit Discovery for Mechanistic Interpretability. In Oh, A.; Naumann, T.; Globerson, A.; Saenko, K.; Hardt, M.; and Levine, S., eds., *Advances in Neural Information Processing Systems 36: Annual Conference on Neural Information Processing Systems 2023, NeurIPS 2023, New Orleans, LA, USA, December 10 - 16, 2023*.
- Elhage, N.; Nanda, N.; Olsson, C.; Henighan, T.; Joseph, N.; Mann, B.; Askell, A.; Bai, Y.; Chen, A.; Conerly, T.; et al. 2021. A mathematical framework for transformer circuits. *Transformer Circuits Thread*, 1(1): 12.
- Farquhar, S.; Kossen, J.; Kuhn, L.; and Gal, Y. 2024. Detecting hallucinations in large language models using semantic entropy. *Nature*, 630(8017): 625–630.
- Ganguli, D.; Lovitt, L.; Kernion, J.; et al. 2022. Red Teaming Language Models to Reduce Harms: Methods, Scaling Behaviors, and Lessons Learned. arXiv:2209.07858.
- Geng, J.; Cai, F.; Wang, Y.; Koepl, H.; Nakov, P.; and Gurevych, I. 2024. A Survey of Confidence Estimation and Calibration in Large Language Models. In Duh, K.; Gomez, H.; and Bethard, S., eds., *Proceedings of the 2024 Conference of the North American Chapter of the Association for Computational Linguistics: Human Language Technologies (Volume 1: Long Papers)*, 6577–6595. Mexico City, Mexico: Association for Computational Linguistics.
- Geng, J.; Li, Q.; Woisetschlaeger, H.; Chen, Z.; Wang, Y.; Nakov, P.; Jacobsen, H.; and Karray, F. 2025. A Comprehensive Survey of Machine Unlearning Techniques for Large Language Models. *CoRR*, abs/2503.01854.
- Goodfellow, I. J.; Shlens, J.; and Szegedy, C. 2015. Explaining and harnessing adversarial examples. In *3rd International Conference on Learning Representations, ICLR 2015*.
- Grattafiori, A.; Dubey, A.; Jauhri, A.; et al. 2024. The Llama 3 Herd of Models. arXiv:2407.21783.
- Gu, T.; Dolan-Gavitt, B.; and Garg, S. 2017. BadNets: Identifying Vulnerabilities in the Machine Learning Model Supply Chain. *CoRR*, abs/1708.06733.
- Huang, Y.; Song, J.; Wang, Z.; Zhao, S.; Chen, H.; Juefei-Xu, F.; and Ma, L. 2025. Look Before You Leap: An Exploratory Study of Uncertainty Analysis for Large Language Models. *IEEE Transactions on Software Engineering*, 51(2): 413–429.
- Iverson, H.; Wang, Y.; Pyatkin, V.; et al. 2023. Camels in a Changing Climate: Enhancing LM Adaptation with Tulu 2. *CoRR*, abs/2311.10702.
- Jiang, A. Q.; Sablayrolles, A.; Mensch, A.; et al. 2023. Mistral 7B. *CoRR*, abs/2310.06825.
- Kadavath, S.; Conerly, T.; Askell, A.; et al. 2022. Language Models (Mostly) Know What They Know. arXiv:2207.05221.
- Karimi, H.; Derr, T.; and Tang, J. 2020. Characterizing the Decision Boundary of Deep Neural Networks. arXiv:1912.11460.
- Karimi, H.; and Tang, J. 2020. Decision Boundary of Deep Neural Networks: Challenges and Opportunities. In *Proceedings of the 13th International Conference on Web Search and Data Mining, WSDM '20*, 919–920. New York, NY, USA: Association for Computing Machinery. ISBN 9781450368223.
- Kuhn, L.; Gal, Y.; and Farquhar, S. 2023. Semantic Uncertainty: Linguistic Invariances for Uncertainty Estimation in Natural Language Generation. In *11th International Conference on Learning Representations, ICLR 2023*.
- Lambert, N.; Morrison, J.; Pyatkin, V.; et al. 2025. Tulu 3: Pushing Frontiers in Open Language Model Post-Training. arXiv:2411.15124.
- Lee, C.; and Landgrebe, D. A. 1997. Decision boundary feature extraction for neural networks. *IEEE Transactions on Neural Networks*, 8(1): 75–83.
- Li, M.; Zhao, Y.; Zhang, W.; Li, S.; Xie, W.; Ng, S.-K.; Chua, T.-S.; and Deng, Y. 2025. Knowledge Boundary of Large Language Models: A Survey. In Che, W.; Nabende, J.; Shutova, E.; and Pilehvar, M. T., eds., *Proceedings of the 63rd Annual Meeting of the Association for Computational Linguistics (Volume 1: Long Papers)*, 5131–5157. Vienna, Austria: Association for Computational Linguistics. ISBN 979-8-89176-251-0.
- Li, Y.; Ding, L.; and Gao, X. 2019. On the Decision Boundary of Deep Neural Networks. arXiv:1808.05385.
- Liang, Z.; Hu, H.; Ye, Q.; Xiao, Y.; and Li, H. 2024. Why Are My Prompts Leaked? Unraveling Prompt Extraction Threats in Customized Large Language Models. *arXiv preprint arXiv:2408.02416*.
- Liang, Z.; Hu, H.; Ye, Q.; Xiao, Y.; and Li, R. 2025. Does Low Rank Adaptation Lead to Lower Robustness against Training-Time Attacks? arXiv:2505.12871.
- Lin, Z.; Trivedi, S.; and Sun, J. 2024. Generating with Confidence: Uncertainty Quantification for Black-box Large Language Models. *Transactions on Machine Learning Research*.

- Liu, S.; Yao, Y.; Jia, J.; et al. 2025a. Rethinking machine unlearning for large language models. *Nat. Mac. Intell.*, 7(2): 181–194.
- Liu, X.; Chen, T.; Da, L.; Chen, C.; Lin, Z.; and Wei, H. 2025b. Uncertainty Quantification and Confidence Calibration in Large Language Models: A Survey. In *Proceedings of the 31st ACM SIGKDD Conference on Knowledge Discovery and Data Mining V.2*, KDD '25, 6107–6117. New York, NY, USA: Association for Computing Machinery. ISBN 9798400714542.
- Madry, A.; Makelov, A.; Schmidt, L.; Tsipras, D.; and Vladu, A. 2018. Towards deep learning models resistant to adversarial attacks. In *6th International Conference on Learning Representations, ICLR 2018*.
- Mayne, H.; Kearns, R. O.; Yang, Y.; Bean, A. M.; Delaney, E.; Russell, C.; and Mahdi, A. 2025. LLMs Don't Know Their Own Decision Boundaries: The Unreliability of Self-Generated Counterfactual Explanations. arXiv:2509.09396.
- Mickisch, D.; Assion, F.; Grebner, F.; Günther, W.; and Motta, M. 2020. Understanding the Decision Boundary of Deep Neural Networks: An Empirical Study. arXiv:2002.01810.
- Radford, A.; Narasimhan, K.; Salimans, T.; Sutskever, I.; et al. 2018. Improving language understanding by generative pre-training. OpenAI technical report.
- Ridder, F.; and Schilling, M. 2025. The HalluRAG Dataset: Detecting Closed-Domain Hallucinations in RAG Applications Using an LLM's Internal States. arXiv:2412.17056.
- Rosenblatt, F. 1958. The perceptron: a probabilistic model for information storage and organization in the brain. *Psychological review*, 65(6): 386–408.
- Sharkey, L.; Chughtai, B.; Batson, J.; et al. 2025. Open Problems in Mechanistic Interpretability. *CoRR*, abs/2501.16496.
- Shorinwa, O.; Mei, Z.; Lidard, J.; Ren, A. Z.; and Majumdar, A. 2025. A Survey on Uncertainty Quantification of Large Language Models: Taxonomy, Open Research Challenges, and Future Directions. *ACM Comput. Surv.*, 58(3).
- Taori, R.; Gulrajani, I.; Zhang, T.; Dubois, Y.; Li, X.; Guestrin, C.; Liang, P.; and Hashimoto, T. B. 2023. Stanford Alpaca: An Instruction-following LLaMA model. [https://github.com/tatsu-lab/stanford\\_alpaca](https://github.com/tatsu-lab/stanford_alpaca).
- Touvron, H.; Martin, L.; Stone, K.; et al. 2023. Llama 2: Open Foundation and Fine-Tuned Chat Models. *CoRR*, abs/2307.09288.
- Tumer, K.; and Ghosh, J. 1996. Analysis of decision boundaries in linearly combined neural classifiers. *Pattern recognition*, 29(2): 341–348.
- Tunstall, L.; Beeching, E.; Lambert, N.; et al. 2023. Zephyr: Direct Distillation of LM Alignment. *CoRR*, abs/2310.16944.
- Wang, K. R.; Variengien, A.; Conmy, A.; Shlegeris, B.; and Steinhardt, J. 2023. Interpretability in the Wild: a Circuit for Indirect Object Identification in GPT-2 Small. In *The Eleventh International Conference on Learning Representations, ICLR 2023, Kigali, Rwanda, May 1-5, 2023*. OpenReview.net.
- Xia, S.; Qin, Y.; Li, X.; et al. 2025a. Generative AI Act II: Test Time Scaling Drives Cognition Engineering. arXiv:2504.13828.
- Xia, Z.; Xu, J.; Zhang, Y.; and Liu, H. 2025b. A Survey of Uncertainty Estimation Methods on Large Language Models. arXiv:2503.00172.
- Yang, A.; Li, A.; Yang, B.; et al. 2025a. Qwen3 Technical Report. arXiv:2505.09388.
- Yang, J.; Tu, J.; Liu, H.; et al. 2025b. BARREL: Boundary-Aware Reasoning for Factual and Reliable LLMs. arXiv:2505.13529.
- Yao, J.; Chien, E.; Du, M.; Niu, X.; Wang, T.; Cheng, Z.; and Yue, X. 2024. Machine Unlearning of Pre-trained Large Language Models. In Ku, L.; Martins, A.; and Srikumar, V., eds., *Proceedings of the 62nd Annual Meeting of the Association for Computational Linguistics (Volume 1: Long Papers), ACL 2024, Bangkok, Thailand, August 11-16, 2024*, 8403–8419. Association for Computational Linguistics.
- Yousefzadeh, R.; and O'Leary, D. P. 2019. Investigating Decision Boundaries of Trained Neural Networks. arXiv:1908.02802.
- Zhang, R.; Lin, L.; Bai, Y.; and Mei, S. 2024. Negative Preference Optimization: From Catastrophic Collapse to Effective Unlearning. *CoRR*, abs/2404.05868.
- Zhao, S.; Nguyen, T.; and Grover, A. 2024. Probing the Decision Boundaries of In-context Learning in Large Language Models. In Globerson, A.; Mackey, L.; Belgrave, D.; Fan, A.; Paquet, U.; Tomczak, J.; and Zhang, C., eds., *Advances in Neural Information Processing Systems*, volume 37, 130408–130432. Curran Associates, Inc.
- Zou, A.; Wang, Z.; Kolter, J. Z.; and Fredrikson, M. 2023. Universal and Transferable Adversarial Attacks on Aligned Language Models. *CoRR*, abs/2307.15043.

## A LLM Usage Statement

AI tools were used for error checking, proofreading, result visualization, and code optimization.

## B Additional Related Work

**Decision Boundary Analysis on ML Models.** The earliest exploration of decision boundaries in neural networks dates back to the era of linear classifiers and shallow architectures. Rosenblatt (1958) introduced the first linear decision boundary for binary classification, where a hyperplane separates input samples into two classes. For shallow feedforward neural networks (FFNNs) with non-linear activations (e.g., sigmoid, ReLU), several works (Lee and Landgrebe 1997; Tumer and Ghosh 1996) quantified how hidden layers enable non-linear decision boundaries. For instance, Lee and Landgrebe (1997) proposed a feature extraction method that maps input data to a space aligned with FFNN decision boundaries, showing that boundary curvature correlates with model capacity and classification accuracy. The connection between the stability of neural network decision boundaries and overall error performance has also been revealed (Tumer and Ghosh 1996) under ensembling. In recent years, researchers extended decision boundary analysis to convolutional neural networks (CNNs) and transformers. Specifically, Goodfellow, Shlens, and Szegedy (2015) revealed a key vulnerability of deep CNNs: their decision boundaries are locally linear in high-dimensional input spaces, making them susceptible to adversarial examples. Then, Madry et al. (2018) further formalized this by proving that robust training (e.g., adversarial training) “smooths” decision boundaries, reducing local linearity and adversarial susceptibility. Similarly, Gu, Dolan-Gavitt, and Garg (2017) focused on backdoor attacks in CNNs, linking them to hidden “trapdoors” in decision boundaries. Such attacks involve planting a small, specific pattern that shifts the boundary and forces misclassification for triggered inputs. Lee and Landgrebe (1997) laid the groundwork by introducing decision boundary feature extraction and highlighting the role of boundaries in characterizing network behavior before deep learning. Later, Yousefzadeh and O’Leary (2019) examined the decision boundaries of trained networks, analyzing how architectural elements (e.g., depth and activation functions) and training data influence boundary shape, complexity, and stability, providing insights into network task performance. Mickisch et al. (2020) conducted an empirical study on deep network boundaries across CV tasks, including image classification and object detection. Through quantitative and qualitative analysis, they explored boundary behavior near correct and misclassified samples and adversarial examples, bridging theory-practice gaps. Similarly, Karimi and Tang (2020) reviewed boundary research challenges such as high input dimensionality, complex architectures, limited visualization tools, and opportunities, including advanced math, innovative visualization, and robustness enhancements. Karimi, Derr, and Tang (2020) complementarily proposed metrics like smoothness, curvature, and class separation to quantify boundaries, enabling cross-model comparisons and standardized analysis for deep learning interpretability.

**Decision Boundary Analysis on LLMs.** Research on LLMs

mainly focuses on exploring how this concept illuminates the decision-making mechanisms and inherent limitations of LLMs. As an example, Zhao, Nguyen, and Grover (2024) probed the decision boundaries of in-context learning in LLMs, shedding light on how contextual information shapes boundary formation and decision outputs. Another work (Mayne et al. 2025) revealed that LLMs lack awareness of their own decision confidences and that self-generated counterfactual explanations are unreliable. With respect to reasoning ability, BARREL (Yang et al. 2025b) designs a boundary-aware reasoning framework to enhance the factual accuracy of LLMs via boundary awareness. However, these preliminary explorations fail to address the core challenges of LLM decision boundary analysis: how to construct decision boundaries for the generalized LLM token generation task (which extends beyond specially designed toy classification tasks) in a computationally feasible manner? how to theoretically analyze the construction error for the decision boundary? To fill this gap, we aim to propose a new decision boundary theory to address the high-dimensional complexity and construction barriers of LLMs, enabling accurate, efficient, and interpretable boundary modeling that aligns with the inherent characteristics of LLMs.

## C Proofs

### C.1 Proof of Theorem 3.2

*Proof. Part I: Proof of Equation 2.*

We aim to characterize the decision boundary  $\mathcal{B}_M^{(f, \mathcal{D})}$  for a neural network  $f : \mathbb{R}^d \rightarrow \mathbb{R}^M$  in the multi-class classification setting ( $M > 2$ ) under an input distribution  $\mathcal{D} \subseteq \mathbb{R}^d$ . The network is decomposed as  $f = \sigma \circ f_{\text{cls}} \circ f_r$ , where:

- $f_r : \mathbb{R}^d \rightarrow \mathbb{R}^{d_h}$  maps the input  $\mathbf{x}$  to a latent representation  $h = f_r(\mathbf{x})$ ,
- $f_{\text{cls}} : \mathbb{R}^{d_h} \rightarrow \mathbb{R}^M$  is a linear classification head,  $f_{\text{cls}}(h) = W_{\text{cls}}h + b_{\text{cls}}$ , with  $W_{\text{cls}} \in \mathbb{R}^{M \times d_h}$ ,  $b_{\text{cls}} \in \mathbb{R}^M$ ,
- $\sigma : \mathbb{R}^M \rightarrow \mathbb{R}^M$  is the softmax function,  $\sigma(z)_i = \frac{e^{z_i}}{\sum_{j=1}^M e^{z_j}}$ , producing probabilities  $P = [p_1, p_2, \dots, p_M]$  with  $\sum_{i=1}^M p_i = 1$ .

By Definition 3.1, the decision boundary  $\mathcal{B}_M^{(f, \mathcal{D})}$  is the set of inputs  $\mathbf{x} \in \mathcal{D}$  such that there exist at least two classes  $m, n \in \mathcal{M} = \{1, 2, \dots, M\}$ ,  $m \neq n$ , with equal and maximal probabilities:

$$p_m = p_n \geq \max_{o \in \mathcal{M} \setminus \{m, n\}} p_o. \quad (16)$$

Since  $\sigma$  is the softmax function,  $p_m = \sigma(z)_m = \frac{e^{z_m}}{\sum_{j=1}^M e^{z_j}}$ , the condition  $p_m = p_n$  implies:

$$\frac{e^{z_m}}{\sum_{j=1}^M e^{z_j}} = \frac{e^{z_n}}{\sum_{j=1}^M e^{z_j}} \implies e^{z_m} = e^{z_n} \implies z_m = z_n. \quad (17)$$

The logits are given by  $z = W_{\text{cls}}h + b_{\text{cls}}$ , so:

$$z_m = w_m h + b_m, \quad z_n = w_n h + b_n, \quad (18)$$

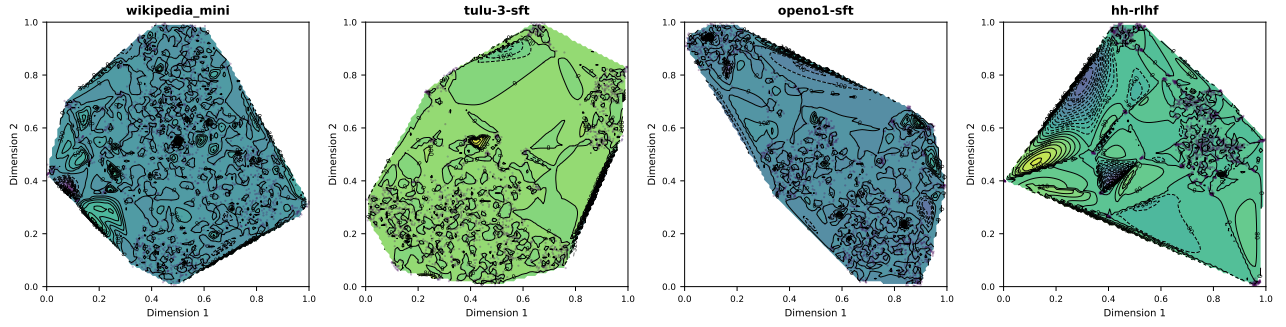


Figure 6: Contour visualization of the  $K$ -DPS ( $K = 2, 500$ ) for Llama-3.2-1B on four datasets. Region colors represent the decision potential values. Black lines denote isohypses, with the 0-isohypse indicating the decision boundary. Cubic interpolation is applied to construct the mesh grid, with visualizations using linear and nearest interpolation shown in Figures 8 and 9.

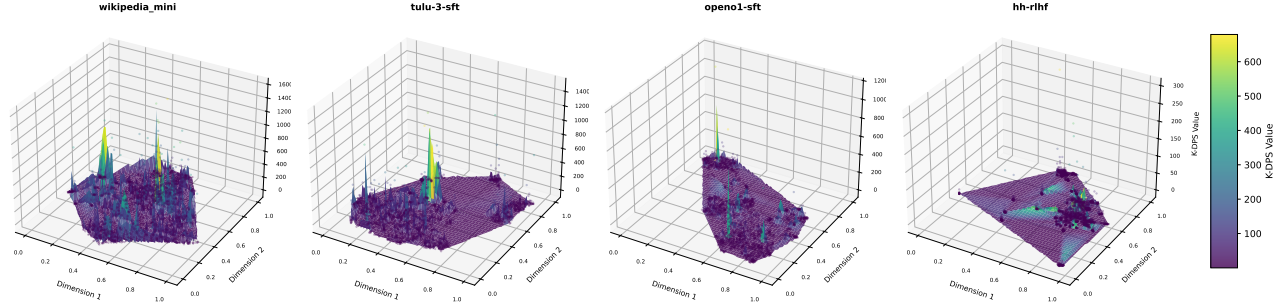


Figure 7: Three-dimensional visualization of the  $K$ -DPS ( $K = 2, 500$ ) for Llama-3.2-1B on four datasets.

where  $w_m, w_n$  are the  $m$ -th and  $n$ -th rows of  $W_{\text{cls}}$ , and  $b_m, b_n$  are the corresponding entries of  $b_{\text{cls}}$ . Thus,  $z_m = z_n$  implies:

$$(w_m - w_n)h + (b_m - b_n) = 0. \quad (19)$$

Additionally, for  $p_m = p_n$  to be maximal, we require  $p_m \geq p_o$  for all  $o \neq m, n$ , which implies:  $\forall o \neq m, n$ ,

$$\frac{e^{z_m}}{\sum_{j=1}^M e^{z_j}} \geq \frac{e^{z_o}}{\sum_{j=1}^M e^{z_j}} \implies e^{z_m} \geq e^{z_o} \implies z_m \geq z_o. \quad (20)$$

Since  $z_m = z_n$ , this becomes:

$$z_m = z_n \geq z_o, \quad \forall o \neq m, n. \quad (21)$$

In the representation space, this translates to:

$$\begin{aligned} (w_m - w_o)h + (b_m - b_o) &\geq 0, \\ (w_n - w_o)h + (b_n - b_o) &\geq 0, \quad \forall o \neq m, n. \end{aligned} \quad (22)$$

For each pair  $m, n \in \mathcal{M}$ ,  $1 \leq m < n \leq M$ , define:

$$\begin{aligned} \mathcal{B}_{mn} &= \{h \in \mathbb{R}^{d_h} \mid (w_m - w_n)h + (b_m - b_n) = 0, \\ & z_m = z_n \geq z_o \forall o \neq m, n, h = f_r(\mathbf{x}), \mathbf{x} \in \mathcal{D}\}. \end{aligned} \quad (23)$$

The decision boundary is the union of all such pairwise boundaries:

$$\mathcal{B}_M^{(f, \mathcal{D})} = \bigcup_{1 \leq m < n \leq M} \mathcal{B}_{mn}. \quad (24)$$

## Part II: Voronoi Cells.

Each  $\mathcal{B}_{mn}$  is a  $(d_h - 1)$ -dimensional hyperplane in  $\mathbb{R}^{d_h}$  defined by  $(w_m - w_n)h + (b_m - b_n) = 0$ , restricted to points where  $z_m = z_n \geq z_o$ . Geometrically, the classification region for class  $i$  is:

$$\begin{aligned} \mathcal{R}_i &= \{h \in \mathbb{R}^{d_h} \mid w_i h + b_i > w_j h + b_j, \\ & \forall j \neq i, h = f_r(\mathbf{x}), \mathbf{x} \in \mathcal{D}\}. \end{aligned} \quad (25)$$

These regions are convex polytopes, as they are defined by the intersection of half-spaces  $(w_i - w_j)h + (b_i - b_j) > 0$ . The boundaries between  $\mathcal{R}_m$  and  $\mathcal{R}_n$  occur where  $(w_m - w_n)h + (b_m - b_n) = 0$  and  $z_m = z_n \geq z_o$ , forming  $\mathcal{B}_{mn}$ . The collection  $\{\mathcal{R}_i\}_{i=1}^M$  partitions the representation space, and the hyperplanes  $\mathcal{B}_{mn}$  form the boundaries of a Voronoi-like partition, where each  $\mathcal{R}_i$  is a Voronoi cell corresponding to class  $i$ .

This completes the proof.  $\square$

## C.2 Proof of Theorem 3.3

*Proof.* We aim to characterize the decision boundary  $\mathcal{B}_{\text{llm}}^{(f, \mathcal{D}')}$  of an LLM  $f : \mathcal{V}^{N_q} \rightarrow \mathcal{V}^{N_r}$  under an input text distribution  $\mathcal{D}' \subseteq \bigcup_{n_q=1}^{N_q} \mathcal{V}^{n_q}$ . The LLM generates a sequence  $\mathbf{y} = [y_1, \dots, y_{N_r}] \in \mathcal{V}^{N_r}$ , where  $\mathcal{V} = \{1, 2, \dots, V\}$  is the vocabulary, conditioned on a prompt  $\mathbf{x} \in \mathcal{D}'$ . The joint probability of generating  $\mathbf{y}$  is:

$$P_f(\mathbf{y} | \mathbf{x}) = \prod_{t=1}^{N_r} P_f(y_t | \mathbf{x}, y_1, \dots, y_{t-1}),$$

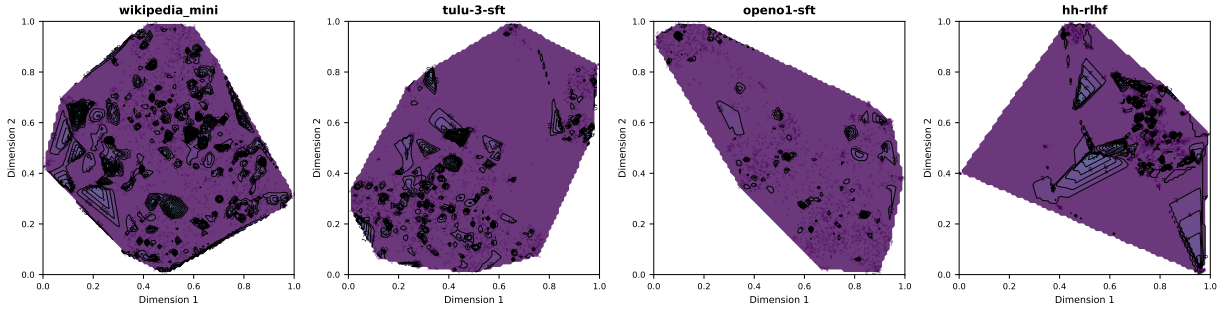


Figure 8: Contour visualization of 2,500-grained decision potential surface for Llama-3.2-1B on four datasets with linear interpolation.

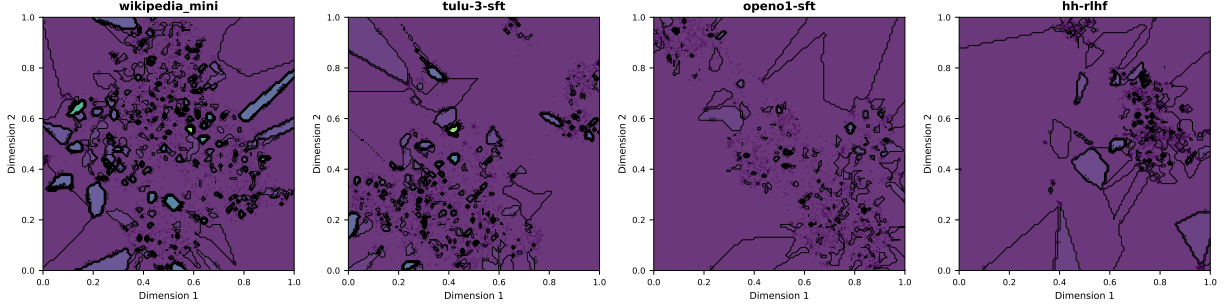


Figure 9: Contour visualization of 2,500-grained decision potential surface of Llama-3.2-1B on four datasets with nearest interpolation.

where  $P_f(y_t|\mathbf{x}, y_1, \dots, y_{t-1})$  is the probability of predicting token  $y_t$  at step  $t$ , modeled as a multi-class classification over  $\mathcal{V}$ .

Based on  $\mathbf{y}^* = \arg \max_{\mathbf{y} \in \mathcal{V}^{N_r}} P_f(\mathbf{y}|\mathbf{x})$  and Definition 3.1, the decision boundary  $\mathcal{B}_{llm}^{(f, \mathcal{D}')}$  is the set of prompts  $\mathbf{x} \in \mathcal{D}'$  where at least two distinct sequences  $\mathbf{y}_v, \mathbf{y}_w \in \mathcal{V}^{N_r}$  have equal and maximal joint probabilities:

$$P_f(\mathbf{y}_v|\mathbf{x}) = P_f(\mathbf{y}_w|\mathbf{x}) \geq \max_{\mathbf{y}_u \in \mathcal{V}^{N_r} \setminus \{\mathbf{y}_v, \mathbf{y}_w\}} P_f(\mathbf{y}_u|\mathbf{x}).$$

For each pair of distinct sequences  $\mathbf{y}_v, \mathbf{y}_w \in \mathcal{V}^{N_r}$ , define:

$$\mathcal{B}_{llm, vw} = \{\mathbf{x} \in \mathcal{D}' \mid P_f(\mathbf{y}_v|\mathbf{x}) = P_f(\mathbf{y}_w|\mathbf{x}) \geq \max_{\mathbf{y}_u \in \mathcal{V}^{N_r} \setminus \{\mathbf{y}_v, \mathbf{y}_w\}} P_f(\mathbf{y}_u|\mathbf{x})\}. \quad (26)$$

The decision boundary is the union over all such pairs:

$$\mathcal{B}_{llm}^{(f, \mathcal{D}')} = \bigcup_{\mathbf{y}_v \neq \mathbf{y}_w \in \mathcal{V}^{N_r}} \mathcal{B}_{llm, vw}.$$

To show this, consider the autoregressive process. For a prompt  $\mathbf{x}$ , the probability  $P_f(\mathbf{y}|\mathbf{x})$  depends on the token probabilities at each step. Obviously, the predicted sequence  $\mathbf{y}^*$  maximizes  $P_f(\mathbf{y}|\mathbf{x})$ . The decision boundary occurs when two sequences  $\mathbf{y}_v$  and  $\mathbf{y}_w$  have equal probabilities, and no

other sequence has a higher probability. This implies:

$$\begin{aligned} P_f(\mathbf{y}_v|\mathbf{x}) &= \prod_{t=1}^{N_r} P_f(y_{v,t}|\mathbf{x}, y_{v,1}, \dots, y_{v,t-1}) \\ &= \prod_{t=1}^{N_r} P_f(y_{w,t}|\mathbf{x}, y_{w,1}, \dots, y_{w,t-1}) \\ &= P_f(\mathbf{y}_w|\mathbf{x}), \end{aligned} \quad (27)$$

and for all  $\mathbf{y}_u \neq \mathbf{y}_v, \mathbf{y}_w$ :

$$P_f(\mathbf{y}_v|\mathbf{x}) \geq P_f(\mathbf{y}_u|\mathbf{x}).$$

Since each token prediction is a multi-class classification (as in Theorem 3.2), the boundary for a single token  $y_t$  is defined by equal probabilities for the top tokens. For the full sequence, the boundary  $\mathcal{B}_{llm, vw}$  corresponds to prompts  $\mathbf{x}$  where the joint probabilities align, which may occur when the log-probabilities differ at some steps but sum to the same value. The maximality condition ensures that  $\mathbf{y}_v$  and  $\mathbf{y}_w$  are the top sequences.

This completes the proof.  $\square$

### C.3 Proof of Theorem 4.4

*Proof.* We aim to prove that the decision boundary  $\mathcal{B}_{llm}^{(f, \mathcal{D}')}$  defined in Theorem 3.3 is equivalent to the 0-isohypse  $\mathcal{D}'_{(0, f)}$  on the decision potential surface  $\mathcal{S}^{(f, \mathcal{D}')}$ , and that the regions separated by this boundary correspond exactly to the Voronoi cells in the token-combined classification definition.

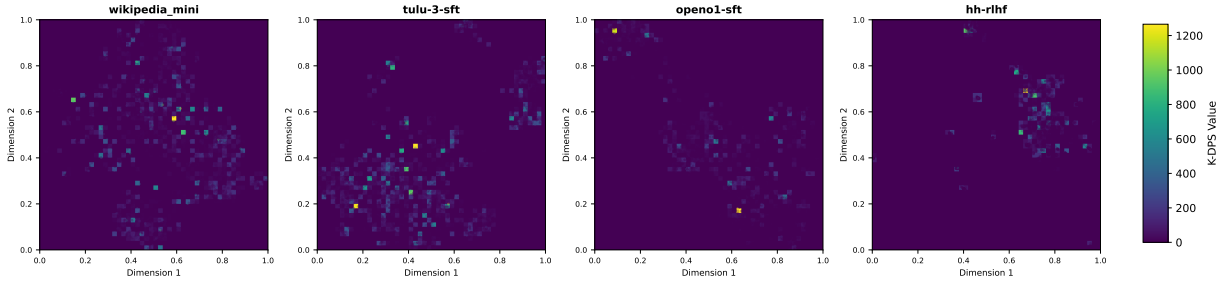


Figure 10: Heatmap visualization of the decision potential surface on four datasets.

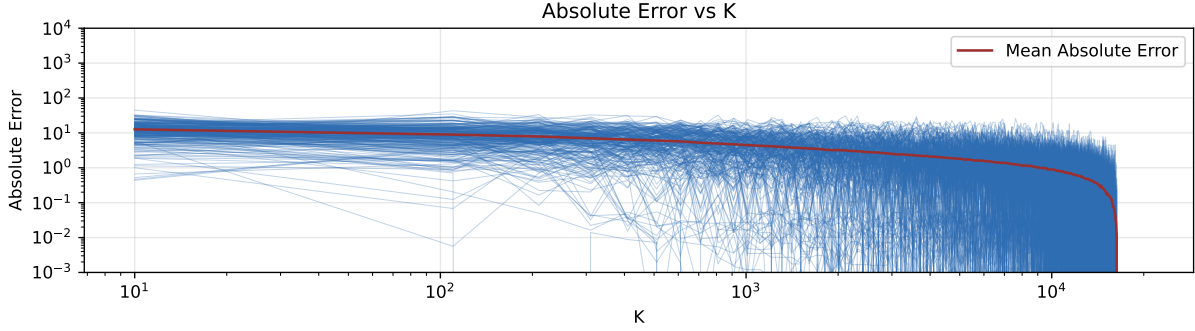


Figure 11: Effect of sampling size  $K$  on the absolute error between the reference  $K$ -DPS (computed with  $K = 20,000$ ) and  $K$ -DPS values for varying  $K$ . Each blue line represents a trend of absolute error across input samples.

Recall from Theorem 3.3 that the decision boundary is

$$\mathcal{B}_{llm}^{(f, \mathcal{D}')} = \bigcup_{\mathbf{y}_v \neq \mathbf{y}_w \in \mathcal{V}^{N_r}} \mathcal{B}_{llm, vw}, \quad (28)$$

where

$$\begin{aligned} \mathcal{B}_{llm, vw} &= \{\mathbf{x} \in \mathcal{D}' \mid \\ P_f(\mathbf{y}_v | \mathbf{x}) = P_f(\mathbf{y}_w | \mathbf{x}) &\geq \max_{\mathbf{y}_u \in \mathcal{V}^{N_r} \setminus \{\mathbf{y}_v, \mathbf{y}_w\}} P_f(\mathbf{y}_u | \mathbf{x})\}. \end{aligned} \quad (29)$$

This boundary consists of prompts  $\mathbf{x}$  where at least two distinct sequences  $\mathbf{y}_v$  and  $\mathbf{y}_w$  have equal and maximal joint probabilities, leading to ambiguity in the predicted output sequence.

From Definition 4.1, the decision potential function is

$$\Phi_f^\infty(\mathbf{x}) = (\log P_f(\mathbf{y}_1 | \mathbf{x}) - \log P_f(\mathbf{y}_2 | \mathbf{x}))^2, \quad (30)$$

where  $\mathbf{y}_1, \mathbf{y}_2 \in \mathcal{V}^{N_r}$  are the sequences with the highest and second-highest log-likelihoods, respectively. The 0-isohypse is defined as

$$\mathcal{D}'_{(0, f)} = \{\mathbf{x} \in \mathcal{D}' \mid \Phi_f^\infty(\mathbf{x}) = 0\}. \quad (31)$$

By definition,  $\Phi_f^\infty(\mathbf{x}) = 0$  if and only if  $\log P_f(\mathbf{y}_1 | \mathbf{x}) = \log P_f(\mathbf{y}_2 | \mathbf{x})$ , which implies  $P_f(\mathbf{y}_1 | \mathbf{x}) = P_f(\mathbf{y}_2 | \mathbf{x})$ . Since  $\mathbf{y}_1$  and  $\mathbf{y}_2$  are the top two sequences by log-likelihood, this equality ensures that

$$P_f(\mathbf{y}_1 | \mathbf{x}) = P_f(\mathbf{y}_2 | \mathbf{x}) \geq P_f(\mathbf{y}_u | \mathbf{x}), \quad \forall \mathbf{y}_u \neq \mathbf{y}_1, \mathbf{y}_2, \quad (32)$$

satisfying the maximality condition in Theorem 3.3. Thus,  $\mathbf{x} \in \mathcal{D}'_{(0, f)}$  if and only if  $\mathbf{x} \in \mathcal{B}_{llm}^{(f, \mathcal{D}')}$ , establishing the set equivalence

$$\mathcal{B}_{llm}^{(f, \mathcal{D}')} = \mathcal{D}'_{(0, f)}. \quad (33)$$

Geometrically, the regions separated by the 0-isohypse are the connected components of  $\mathcal{D}' \setminus \mathcal{D}'_{(0, f)}$ , where each region corresponds to prompts for which a unique sequence  $\mathbf{y}_i$  has the highest log-likelihood ( $\Phi_f^\infty(\mathbf{x}) > 0$ ). These regions are exactly the Voronoi cells in the sequence-level classification framework of Theorem 3.3, as each cell consists of prompts yielding the same maximal sequence. The 0-isohypse forms the boundaries between these cells, partitioning the prompt space  $\mathcal{D}'$  into regions of unambiguous predictions.

This completes the proof.  $\square$

#### C.4 Proof of Corollary 4.5

*Proof.* We aim to show that for any  $\varepsilon > 0$ , the input space  $\mathcal{D}'$  is partitioned into three disjoint strata based on the value of the decision potential function  $\Phi_f^\infty(\mathbf{x})$ :

$$\mathcal{D}' = \mathcal{D}'_{(>\varepsilon, f)} \sqcup \mathcal{D}'_{(<\varepsilon, f)} \sqcup \mathcal{D}'_{(\varepsilon, f)}, \quad (34)$$

where  $\sqcup$  denotes disjoint union.

From Definition 4.3, the  $\varepsilon$ -isohypse is

$$\mathcal{D}'_{(\varepsilon, f)} = \{\mathbf{x} \in \mathcal{D}' \mid \Phi_f^\infty(\mathbf{x}) = \varepsilon\}, \quad (35)$$

and the other strata are defined as

$$\begin{aligned} \mathcal{D}'_{(>\varepsilon, f)} &= \{\mathbf{x} \in \mathcal{D}' \mid \Phi_f^\infty(\mathbf{x}) > \varepsilon\}, \\ \mathcal{D}'_{(<\varepsilon, f)} &= \{\mathbf{x} \in \mathcal{D}' \mid \Phi_f^\infty(\mathbf{x}) < \varepsilon\}. \end{aligned} \quad (36)$$

Since  $\Phi_f^\infty : \mathcal{D}' \rightarrow \mathbb{R}_+$  is a continuous function (assuming log-likelihoods are continuous in the prompt space), these sets are disjoint and their union covers  $\mathcal{D}'$ .

- $\varepsilon$ -confident regions: For  $\mathbf{x} \in \mathcal{D}'_{(>\varepsilon, f)}$ ,  $\Phi_f^\infty(\mathbf{x}) > \varepsilon$ , so

$$|\log P_f(\mathbf{y}_1|\mathbf{x}) - \log P_f(\mathbf{y}_2|\mathbf{x})| > \sqrt{\varepsilon}. \quad (37)$$

Since  $\mathbf{y}_1$  has the highest log-likelihood,  $\log P_f(\mathbf{y}_1|\mathbf{x}) - \log P_f(\mathbf{y}_2|\mathbf{x}) > \sqrt{\varepsilon}$ , meaning the model predicts  $\mathbf{y}_1$  with at least  $\sqrt{\varepsilon}$  nats (natural units of information) of confidence over the next most likely sequence  $\mathbf{y}_2$ .

- $\varepsilon$ -uncertain regions: For  $\mathbf{x} \in \mathcal{D}'_{(<\varepsilon, f)}$ ,  $\Phi_f^\infty(\mathbf{x}) < \varepsilon$ , so

$$|\log P_f(\mathbf{y}_1|\mathbf{x}) - \log P_f(\mathbf{y}_2|\mathbf{x})| < \sqrt{\varepsilon}. \quad (38)$$

Here, the model has low confidence, with a margin less than  $\sqrt{\varepsilon}$  nats between the top two sequences. As  $\varepsilon \rightarrow 0$ ,  $\Phi_f^\infty(\mathbf{x}) \rightarrow 0$ , so  $\mathcal{D}'_{(<\varepsilon, f)}$  converges to the 0-isohypse  $\mathcal{D}'_{(0, f)}$ , where the margin is zero.

- $\varepsilon$ -isohypse: For  $\mathbf{x} \in \mathcal{D}'_{(\varepsilon, f)}$ ,  $\Phi_f^\infty(\mathbf{x}) = \varepsilon$ , so the confidence margin is exactly  $\sqrt{\varepsilon}$  nats, forming the contour that separates confident and uncertain regions.

The disjointness of the strata follows from the strict inequalities and equality defining them, and their union covers  $\mathcal{D}'$  since  $\Phi_f^\infty(\mathbf{x}) \geq 0$  for all  $\mathbf{x} \in \mathcal{D}'$ .

This completes the proof.  $\square$

## C.5 Proof of Theorem 4.7

*Proof.* Let  $\mathbf{x} \in \mathcal{D}'$  be a fixed input, and let  $\mathcal{Y}_K = \{\mathbf{y}_1, \mathbf{y}_2, \dots, \mathbf{y}_K\}$  be a set of  $K$  i.i.d. samples drawn from the language model's output distribution  $P_f(\cdot|\mathbf{x})$ . The decision potential function is:

$$\Phi_f^\infty(\mathbf{x}) = (\log P_f(\mathbf{y}_{1*}|\mathbf{x}) - \log P_f(\mathbf{y}_{2*}|\mathbf{x}))^2, \quad (39)$$

where  $\mathbf{y}_{1*}$  and  $\mathbf{y}_{2*}$  are the top two generated texts with the highest log-likelihoods over the entire output space  $\mathcal{Y}^{N_r}$ , and

$$\Phi_f^K(\mathbf{x}) = (\log P_f(\mathbf{y}_{1*}^K|\mathbf{x}) - \log P_f(\mathbf{y}_{2*}^K|\mathbf{x}))^2, \quad (40)$$

where  $\mathbf{y}_{1*}^K$  and  $\mathbf{y}_{2*}^K$  are the top two generated texts within  $\mathcal{Y}_K$ . We aim to bound the error  $|\Phi_f^K(\mathbf{x}) - \Phi_f^\infty(\mathbf{x})|$  with probability at least  $1 - \delta - 2\varepsilon_{\text{tail}}$  for  $\delta \in (0, 1)$ .

**Step 1: Preliminary.** Define:

$$\begin{aligned} \Delta_\infty(\mathbf{x}) &= \log P_f(\mathbf{y}_{1*}|\mathbf{x}) - \log P_f(\mathbf{y}_{2*}|\mathbf{x}), \\ \Delta_K(\mathbf{x}) &= \log P_f(\mathbf{y}_{1*}^K|\mathbf{x}) - \log P_f(\mathbf{y}_{2*}^K|\mathbf{x}). \end{aligned} \quad (41)$$

Thus,  $\Phi_f^\infty(\mathbf{x}) = (\Delta_\infty(\mathbf{x}))^2$  and  $\Phi_f^K(\mathbf{x}) = (\Delta_K(\mathbf{x}))^2$ . The error can be expressed as:

$$\begin{aligned} &|\Phi_f^K(\mathbf{x}) - \Phi_f^\infty(\mathbf{x})| \\ &= |(\Delta_K(\mathbf{x}))^2 - (\Delta_\infty(\mathbf{x}))^2| \\ &= |\Delta_K(\mathbf{x}) - \Delta_\infty(\mathbf{x})| \cdot |\Delta_K(\mathbf{x}) + \Delta_\infty(\mathbf{x})|. \end{aligned} \quad (42)$$

Since  $\mathcal{Y}_K$  is finite,  $\mathbf{y}_{1*}^K$  and  $\mathbf{y}_{2*}^K$  are the top-2 outputs in  $\mathcal{Y}_K$ , which may not include  $\mathbf{y}_{1*}$  or  $\mathbf{y}_{2*}$ . Define:

$$R_K(\mathbf{x}) = \log P_f(\mathbf{y}_{1*}^K|\mathbf{x}) - \min_{\mathbf{y} \in \mathcal{Y}_K} \log P_f(\mathbf{y}|\mathbf{x}), \quad (43)$$

which represents the *diameter* of log-likelihoods in  $\mathcal{Y}_K$ .

**Lemma C.1** ( $\Pr(\mathbf{y}_{1*} \notin \mathcal{Y}_K) \leq \varepsilon_{\text{tail}}$ ). *Define the tail probability  $\varepsilon_{\text{tail}}$  as:  $\varepsilon_{\text{tail}} = (1 - P_f(\mathbf{y}_{1*}^K|\mathbf{x}))^K$ . Then, we have  $\Pr(\mathbf{y}_{1*} \notin \mathcal{Y}_K) \leq \varepsilon_{\text{tail}}$ .*

*A short proof of Lemma C.1:* As  $\mathbf{y}_k \in \mathcal{Y}_K$  are i.i.d., we know that with  $K$  samples of  $\mathbf{y} \sim P_f(\cdot|\mathbf{x})$  the probability that we cannot obtain  $\mathbf{y}_{1*}$  obeys a geometric distribution, i.e.,

$$\Pr(\mathbf{y}_{1*} \notin \mathcal{Y}_K) = (1 - P_f(\mathbf{y}_{1*}|\mathbf{x}))^K. \quad (44)$$

As  $P_f(\mathbf{y}_{1*}|\mathbf{x}) \geq P_f(\mathbf{y}_{1*}^K|\mathbf{x})$ , then we have

$$\begin{aligned} &\Pr(\mathbf{y}_{1*} \notin \mathcal{Y}_K) \\ &= (1 - P_f(\mathbf{y}_{1*}|\mathbf{x}))^K \leq (1 - P_f(\mathbf{y}_{1*}^K|\mathbf{x}))^K = \varepsilon_{\text{tail}}, \end{aligned} \quad (45)$$

which ends the proof.

Based on Lemma C.1, we know that  $\varepsilon_{\text{tail}}$  bounds the probability that the true top output  $\mathbf{y}_{1*}$  is not included in  $\mathcal{Y}_K$ .

**Step 2: Bounding  $|\Delta_K(\mathbf{x}) - \Delta_\infty(\mathbf{x})|$ .**

Since  $\Delta_K(\mathbf{x})$  is computed over a random sample, we consider using *concentration inequalities* to bound the deviation  $|\Delta_K(\mathbf{x}) - \Delta_\infty(\mathbf{x})|$ . The log-likelihoods  $\log P_f(\mathbf{y}_k|\mathbf{x})$  for  $\mathbf{y}_k \in \mathcal{Y}_K$  are i.i.d., and they are bounded within the diameter  $R_K(\mathbf{x})$ . By *Hoeffding's inequality*, the deviation of the sample maximum log-likelihood from its expected maximum is bounded. Specifically, for the top-1 log-likelihood  $\forall t > 0$ , we have:

$$\Pr\left(\left|\log P_f(\mathbf{y}_{1*}^K|\mathbf{x}) - \log P_f(\mathbf{y}_{1*}|\mathbf{x})\right| > t\right) \leq 2 \exp\left(-\frac{2Kt^2}{R_K^2(\mathbf{x})}\right). \quad (46)$$

Similarly, for the second-highest log-likelihood, a similar bound applies.

Combining these, we have:

$$\begin{aligned} &|\Delta_K(\mathbf{x}) - \Delta_\infty(\mathbf{x})| \\ &= |(\log P_f(\mathbf{y}_{1*}^K|\mathbf{x}) - \log P_f(\mathbf{y}_{2*}^K|\mathbf{x})) - (\log P_f(\mathbf{y}_{1*}|\mathbf{x}) - \log P_f(\mathbf{y}_{2*}|\mathbf{x}))| \\ &= |(\log P_f(\mathbf{y}_{1*}^K|\mathbf{x}) - \log P_f(\mathbf{y}_{1*}|\mathbf{x})) - (\log P_f(\mathbf{y}_{2*}^K|\mathbf{x}) - \log P_f(\mathbf{y}_{2*}|\mathbf{x}))|. \end{aligned} \quad (47)$$

Based on the triangle inequality  $|a - b| \leq |a| + |b|$  when  $a, b \in \mathbb{R}$ , we know that

$$\begin{aligned} &|\Delta_K(\mathbf{x}) - \Delta_\infty(\mathbf{x})| \\ &= |(\log P_f(\mathbf{y}_{1*}^K|\mathbf{x}) - \log P_f(\mathbf{y}_{1*}|\mathbf{x})) - (\log P_f(\mathbf{y}_{2*}^K|\mathbf{x}) - \log P_f(\mathbf{y}_{2*}|\mathbf{x}))| \\ &\leq |\log P_f(\mathbf{y}_{1*}^K|\mathbf{x}) - \log P_f(\mathbf{y}_{1*}|\mathbf{x})| + |\log P_f(\mathbf{y}_{2*}^K|\mathbf{x}) - \log P_f(\mathbf{y}_{2*}|\mathbf{x})|. \end{aligned} \quad (48)$$

To bound  $|\Delta_K(\mathbf{x}) - \Delta_\infty(\mathbf{x})|$ , we aim to find the maximal probability for the event  $|\Delta_K(\mathbf{x}) - \Delta_\infty(\mathbf{x})| < t'$  with  $t' > 0$ . Without losing generality, we set  $t' = 2t$ , where the objective can be reformulated as:

$$\begin{aligned} &\Pr(|\Delta_K(\mathbf{x}) - \Delta_\infty(\mathbf{x})| < t') \\ &= 1 - \Pr(|\Delta_K(\mathbf{x}) - \Delta_\infty(\mathbf{x})| \geq t'), \end{aligned} \quad (49)$$

where

$$\begin{aligned}
& \Pr(|\Delta_K(\mathbf{x}) - \Delta_\infty(\mathbf{x})| \geq t') \\
&= \Pr(|\log P_f(\mathbf{y}_{1*}^K|\mathbf{x}) - \log P_f(\mathbf{y}_{1*}|\mathbf{x})| \geq t \\
&\quad \text{or } |\log P_f(\mathbf{y}_{2*}^K|\mathbf{x}) - \log P_f(\mathbf{y}_{2*}|\mathbf{x})| \geq t)) \\
&\leq \Pr(|\log P_f(\mathbf{y}_{1*}^K|\mathbf{x}) - \log P_f(\mathbf{y}_{1*}|\mathbf{x})| \geq t) + \\
&\quad \Pr(|\log P_f(\mathbf{y}_{2*}^K|\mathbf{x}) - \log P_f(\mathbf{y}_{2*}|\mathbf{x})| \geq t) \quad (50) \\
&\leq 2 \exp\left(-\frac{2Kt^2}{R_K^2(\mathbf{x})}\right) + 2 \exp\left(-\frac{2Kt^2}{R_K^2(\mathbf{x})}\right) \\
&= 4 \exp\left(-\frac{2Kt^2}{R_K^2(\mathbf{x})}\right).
\end{aligned}$$

So we have

$$\begin{aligned}
& \Pr(|\Delta_K(\mathbf{x}) - \Delta_\infty(\mathbf{x})| < t') \\
&= 1 - \Pr(|\Delta_K(\mathbf{x}) - \Delta_\infty(\mathbf{x})| \geq t') \quad (51) \\
&\geq 1 - 4 \exp\left(-\frac{2Kt^2}{R_K^2(\mathbf{x})}\right).
\end{aligned}$$

Suppose we have at least  $1 - \delta$  probability to support this event stands, we have

$$\begin{aligned}
& 1 - 4 \exp\left(-\frac{2Kt^2}{R_K^2(\mathbf{x})}\right) \geq 1 - \delta \\
&\Leftrightarrow 4 \exp\left(-\frac{2Kt^2}{R_K^2(\mathbf{x})}\right) \leq \delta \\
&\Leftrightarrow \exp\left(-\frac{2Kt^2}{R_K^2(\mathbf{x})}\right) \leq \frac{\delta}{4} \\
&\Leftrightarrow -\frac{2Kt^2}{R_K^2(\mathbf{x})} \leq \log \frac{\delta}{4} \\
&\Leftrightarrow \frac{2Kt^2}{R_K^2(\mathbf{x})} \geq -\log \frac{\delta}{4} \quad (52) \\
&\Leftrightarrow \frac{2Kt^2}{R_K^2(\mathbf{x})} \geq \log \frac{4}{\delta} \\
&\Leftrightarrow t^2 \geq \frac{R_K^2(\mathbf{x})}{2K} \log \frac{4}{\delta} \\
&\Leftrightarrow t \geq |R_K(\mathbf{x}) \sqrt{\frac{\log(4/\delta)}{2K}}| \\
&\Leftrightarrow t \geq R_K(\mathbf{x}) \sqrt{\frac{\log(4/\delta)}{2K}}.
\end{aligned}$$

In other words,  $\forall t > 0$  we bound  $\Pr(|\Delta_K(\mathbf{x}) - \Delta_\infty(\mathbf{x})| < t)$  with probability at least  $1 - \delta$  when:

$$t = R_K(\mathbf{x}) \sqrt{\frac{\log(4/\delta)}{2K}}. \quad (53)$$

**Step 3: Bounding  $|\Delta_K(\mathbf{x}) + \Delta_\infty(\mathbf{x})|$ .**

**Assumption C.2** (Bounded Population Gap). There exists a constant  $M > 0$  such that for any  $\mathbf{x}$ , the population top-2 gap satisfies:

$$\Delta_\infty(\mathbf{x}) = \log P_f(\mathbf{y}_{1*}|\mathbf{x}) - \log P_f(\mathbf{y}_{2*}|\mathbf{x}) \leq M \quad (54)$$

Then we assume that

$$M \leq R_K(\mathbf{x}) \quad (55)$$

when  $K \gg 1$ .

This assumption is reasonable as most practical language models do not have extremely large differences between top-2 probabilities, and the probability differences between top-2 would be much smaller than the range of between the top-1 and the sample with the minimal probability in the sampling set. Now we can obtain that:

$$|\Delta_K(\mathbf{x}) + \Delta_\infty(\mathbf{x})| \leq |\Delta_K(\mathbf{x})| + |\Delta_\infty(\mathbf{x})| \leq 2 \cdot R_K(\mathbf{x}). \quad (56)$$

**Step 4: Final bound.**

Define the events

$$\begin{aligned}
A &= \{\mathbf{y}_{1*} \in \mathcal{Y}_K \text{ and } \mathbf{y}_{2*} \in \mathcal{Y}_K\}, \\
B &= \{\mathbf{y}_{1*} \notin \mathcal{Y}_K \text{ or } \mathbf{y}_{2*} \notin \mathcal{Y}_K\}. \quad (57)
\end{aligned}$$

Lemma C.1 and a union bound give

$$\Pr(B) \leq 2\varepsilon_{\text{tail}}. \quad (58)$$

- On event  $A$  we have  $\mathbf{y}_{1*}^K = \mathbf{y}_{1*}$  and  $\mathbf{y}_{2*}^K = \mathbf{y}_{2*}$ , hence

$$\Phi_f^K(\mathbf{x}) = \Phi_f^\infty(\mathbf{x}) \implies |\Phi_f^K(\mathbf{x}) - \Phi_f^\infty(\mathbf{x})| = 0. \quad (59)$$

- On event  $B$  we use the worst-case gap

$$\begin{aligned}
& |\Phi_f^K(\mathbf{x}) - \Phi_f^\infty(\mathbf{x})| \\
&\leq |\Delta_K(\mathbf{x}) - \Delta_\infty(\mathbf{x})| \cdot |\Delta_K(\mathbf{x}) + \Delta_\infty(\mathbf{x})| \\
&\leq R_K(\mathbf{x}) \sqrt{\frac{\log(4/\delta)}{2K}} \cdot 2R_K(\mathbf{x}) \quad (60) \\
&= 2R_K^2(\mathbf{x}) \sqrt{\frac{\log(4/\delta)}{2K}}.
\end{aligned}$$

This completes the proof.  $\square$

## C.6 Proof of Theorem 4.8

*Proof.* Fix an input  $\mathbf{x} \in \mathcal{D}'$ . Recall that

$$\Delta_\infty(\mathbf{x}) = \log P_f(\mathbf{y}_{1*}|\mathbf{x}) - \log P_f(\mathbf{y}_{2*}|\mathbf{x}) \quad (61)$$

and  $\Phi_f^\infty(\mathbf{x}) = \Delta_\infty^2(\mathbf{x})$ .

For  $\eta \geq 0$ , define

$$\begin{aligned}
\mathcal{Y}_{2,\eta}(\mathbf{x}) &= \{\mathbf{y} \in \mathcal{V}^{N_r} : \mathbf{y} \neq \mathbf{y}_{1*}, \\
&\quad \log P_f(\mathbf{y}|\mathbf{x}) \geq \log P_f(\mathbf{y}_{2*}|\mathbf{x}) - \eta\}. \quad (62)
\end{aligned}$$

and define

$$p_{2,\eta}(\mathbf{x}) = \sum_{\mathbf{y} \in \mathcal{Y}_{2,\eta}(\mathbf{x})} P_f(\mathbf{y}|\mathbf{x}). \quad (63)$$

Consider the candidate-discovery event

$$E_\eta = \{\mathbf{y}_{1*} \in \mathcal{Y}_K\} \cap \{\mathcal{Y}_K \cap \mathcal{Y}_{2,\eta}(\mathbf{x}) \neq \emptyset\}. \quad (64)$$

On this event, the sample contains a population top-1 sequence, so the maximal sampled log-likelihood equals the population maximal log-likelihood:

$$\log P_f(\mathbf{y}_{1*}^K|\mathbf{x}) = \log P_f(\mathbf{y}_{1*}|\mathbf{x}). \quad (65)$$

This statement is about the log-likelihood value; if several sequences tie for the top probability,  $\mathbf{y}_{1*}^K$  may be any maximizer in  $\mathcal{Y}_K$ .

Moreover, because  $\mathcal{Y}_K$  contains at least one candidate from  $\mathcal{Y}_{2,\eta}(\mathbf{x})$ , the sampled second-best candidate has log-likelihood at least  $\log P_f(\mathbf{y}_{2*}|\mathbf{x}) - \eta$ :

$$\log P_f(\mathbf{y}_{2*}^K|\mathbf{x}) \geq \log P_f(\mathbf{y}_{2*}|\mathbf{x}) - \eta. \quad (66)$$

At the same time,  $\mathbf{y}_{2*}$  is the second element in the population ordering by log-likelihood. Therefore the second-largest log-likelihood in any sampled subset cannot exceed the population second-largest log-likelihood:

$$\log P_f(\mathbf{y}_{2*}^K|\mathbf{x}) \leq \log P_f(\mathbf{y}_{2*}|\mathbf{x}). \quad (67)$$

Combining the two inequalities gives

$$0 \leq \log P_f(\mathbf{y}_{2*}|\mathbf{x}) - \log P_f(\mathbf{y}_{2*}^K|\mathbf{x}) \leq \eta. \quad (68)$$

Therefore

$$\begin{aligned} \Delta_K(\mathbf{x}) - \Delta_\infty(\mathbf{x}) &= (\log P_f(\mathbf{y}_{1*}^K|\mathbf{x}) - \log P_f(\mathbf{y}_{2*}^K|\mathbf{x})) \\ &\quad - (\log P_f(\mathbf{y}_{1*}|\mathbf{x}) - \log P_f(\mathbf{y}_{2*}|\mathbf{x})) \\ &= \log P_f(\mathbf{y}_{2*}|\mathbf{x}) - \log P_f(\mathbf{y}_{2*}^K|\mathbf{x}), \end{aligned} \quad (69)$$

and hence

$$0 \leq \Delta_K(\mathbf{x}) - \Delta_\infty(\mathbf{x}) \leq \eta. \quad (70)$$

The squared-potential error on  $E_\eta$  is then

$$\begin{aligned} &|\Phi_f^K(\mathbf{x}) - \Phi_f^\infty(\mathbf{x})| \\ &= |\Delta_K^2(\mathbf{x}) - \Delta_\infty^2(\mathbf{x})| \\ &= (\Delta_K(\mathbf{x}) - \Delta_\infty(\mathbf{x}))(\Delta_K(\mathbf{x}) + \Delta_\infty(\mathbf{x})) \\ &\leq \eta((\Delta_\infty(\mathbf{x}) + \eta) + \Delta_\infty(\mathbf{x})) \\ &= \eta(2\Delta_\infty(\mathbf{x}) + \eta). \end{aligned} \quad (71)$$

It remains to lower-bound the probability of  $E_\eta$ . By a union bound,

$$\Pr(E_\eta^c) \leq \Pr(\mathbf{y}_{1*} \notin \mathcal{Y}_K) + \Pr(\mathcal{Y}_K \cap \mathcal{Y}_{2,\eta}(\mathbf{x}) = \emptyset). \quad (72)$$

Since the  $K$  samples are independent,

$$\Pr(\mathbf{y}_{1*} \notin \mathcal{Y}_K) = (1 - P_f(\mathbf{y}_{1*}|\mathbf{x}))^K \quad (73)$$

and

$$\Pr(\mathcal{Y}_K \cap \mathcal{Y}_{2,\eta}(\mathbf{x}) = \emptyset) = (1 - p_{2,\eta}(\mathbf{x}))^K. \quad (74)$$

Thus,

$$\Pr(E_\eta) \geq 1 - (1 - P_f(\mathbf{y}_{1*}|\mathbf{x}))^K - (1 - p_{2,\eta}(\mathbf{x}))^K, \quad (75)$$

which proves Equations (11) and (12).

Finally, suppose  $p_{2,\eta}(\mathbf{x}) > 0$ . Using  $(1 - u)^K \leq \exp(-Ku)$  for  $u \in [0, 1]$ , the two failure terms are each at most  $\delta/2$  whenever

$$K \geq \max \left\{ \frac{\log(2/\delta)}{P_f(\mathbf{y}_{1*}|\mathbf{x})}, \frac{\log(2/\delta)}{p_{2,\eta}(\mathbf{x})} \right\}. \quad (76)$$

Under this sufficient condition,  $\Pr(E_\eta) \geq 1 - \delta$ .  $\square$

## C.7 Proof of Theorem 4.9

*Proof.* We aim to bound the expected error  $\mathbb{E}[|\Phi_f^K(\mathbf{x}) - \Phi_f^\infty(\mathbf{x})|]$  for a fixed input  $\mathbf{x} \in \mathcal{D}'$  and a set  $\mathcal{Y}_K = \{\mathbf{y}_1, \mathbf{y}_2, \dots, \mathbf{y}_K\}$  of  $K$  *i.i.d.* samples drawn from the language model's output distribution  $P_f(\cdot|\mathbf{x})$ . Recall that:

$$\begin{aligned} \Phi_f^\infty(\mathbf{x}) &= (\log P_f(\mathbf{y}_{1*}|\mathbf{x}) - \log P_f(\mathbf{y}_{2*}|\mathbf{x}))^2, \\ \Phi_f^K(\mathbf{x}) &= (\log P_f(\mathbf{y}_{1*}^K|\mathbf{x}) - \log P_f(\mathbf{y}_{2*}^K|\mathbf{x}))^2, \end{aligned} \quad (77)$$

where  $\mathbf{y}_{1*}, \mathbf{y}_{2*}$  are the top-2 outputs over the entire output space  $\mathcal{V}^{N_r}$ , and  $\mathbf{y}_{1*}^K, \mathbf{y}_{2*}^K$  are the top-2 outputs in  $\mathcal{Y}_K$ . Define:

$$\begin{aligned} \Delta_\infty(\mathbf{x}) &= \log P_f(\mathbf{y}_{1*}|\mathbf{x}) - \log P_f(\mathbf{y}_{2*}|\mathbf{x}), \\ \Delta_K(\mathbf{x}) &= \log P_f(\mathbf{y}_{1*}^K|\mathbf{x}) - \log P_f(\mathbf{y}_{2*}^K|\mathbf{x}), \end{aligned} \quad (78)$$

so that  $\Phi_f^\infty(\mathbf{x}) = (\Delta_\infty(\mathbf{x}))^2$ ,  $\Phi_f^K(\mathbf{x}) = (\Delta_K(\mathbf{x}))^2$ , and the error is:

$$\begin{aligned} &|\Phi_f^K(\mathbf{x}) - \Phi_f^\infty(\mathbf{x})| \\ &= |(\Delta_K(\mathbf{x}))^2 - (\Delta_\infty(\mathbf{x}))^2| \\ &= |\Delta_K(\mathbf{x}) - \Delta_\infty(\mathbf{x})| \cdot |\Delta_K(\mathbf{x}) + \Delta_\infty(\mathbf{x})|. \end{aligned} \quad (79)$$

By Assumption C.2,  $|\Delta_\infty(\mathbf{x})| \leq R_K(\mathbf{x})$ , where  $R_K(\mathbf{x}) = \log P_f(\mathbf{y}_{1*}^K|\mathbf{x}) - \min_{\mathbf{y} \in \mathcal{Y}_K} \log P_f(\mathbf{y}|\mathbf{x})$  is the log-likelihood diameter of  $\mathcal{Y}_K$ . Also,  $|\Delta_K(\mathbf{x})| \leq R_K(\mathbf{x})$ , so:

$$|\Delta_K(\mathbf{x}) + \Delta_\infty(\mathbf{x})| \leq |\Delta_K(\mathbf{x})| + |\Delta_\infty(\mathbf{x})| \leq 2R_K(\mathbf{x}). \quad (80)$$

Thus, the error is bounded by:

$$|\Phi_f^K(\mathbf{x}) - \Phi_f^\infty(\mathbf{x})| \leq |\Delta_K(\mathbf{x}) - \Delta_\infty(\mathbf{x})| \cdot 2R_K(\mathbf{x}). \quad (81)$$

We compute the expectation:

$$\mathbb{E}[|\Phi_f^K(\mathbf{x}) - \Phi_f^\infty(\mathbf{x})|] \leq 2R_K(\mathbf{x}) \cdot \mathbb{E}[|\Delta_K(\mathbf{x}) - \Delta_\infty(\mathbf{x})|]. \quad (82)$$

Define  $Z = |\Delta_K(\mathbf{x}) - \Delta_\infty(\mathbf{x})|$ . From the proof of Theorem 4.7 (Equation 50), Hoeffding's inequality gives:

$$\Pr(Z \geq t) \leq 4 \exp\left(-\frac{2Kt^2}{R_K^2(\mathbf{x})}\right). \quad (83)$$

The expectation of  $Z$  is:

$$\mathbb{E}[Z] = \int_0^\infty \Pr(Z \geq t) dt \leq \int_0^\infty 4 \exp\left(-\frac{2Kt^2}{R_K^2(\mathbf{x})}\right) dt. \quad (84)$$

Substitute  $u = \frac{2Kt^2}{R_K^2(\mathbf{x})}$ , so  $t = R_K(\mathbf{x})\sqrt{\frac{u}{2K}}$ ,  $dt = \frac{R_K(\mathbf{x})}{2\sqrt{2K}\sqrt{u}} du$ . Then:

$$\mathbb{E}[Z] \leq \int_0^\infty 4e^{-u} \cdot \frac{R_K(\mathbf{x})}{2\sqrt{2K}\sqrt{u}} du = \frac{2R_K(\mathbf{x})}{\sqrt{2K}} \int_0^\infty \frac{e^{-u}}{\sqrt{u}} du. \quad (85)$$

Since  $\int_0^\infty \frac{e^{-u}}{\sqrt{u}} du = \Gamma\left(\frac{1}{2}\right) = \sqrt{\pi}$ , we have:

$$\mathbb{E}[Z] \leq \frac{2R_K(\mathbf{x})}{\sqrt{2K}} \cdot \sqrt{\pi} = R_K(\mathbf{x})\sqrt{\frac{2\pi}{K}}. \quad (86)$$

Thus:

$$\begin{aligned} & \mathbb{E}[|\Phi_f^K(\mathbf{x}) - \Phi_f^\infty(\mathbf{x})|] \\ & \leq 2R_K(\mathbf{x}) \cdot R_K(\mathbf{x}) \sqrt{\frac{2\pi}{K}} \\ & = 2R_K^2(\mathbf{x}) \sqrt{\frac{2\pi}{K}}. \end{aligned} \quad (87)$$

To account for event  $B = \{\mathbf{y}_{1*} \notin \mathcal{Y}_K \text{ or } \mathbf{y}_{2*} \notin \mathcal{Y}_K\}$  with  $\Pr(B) \leq 2\varepsilon_{\text{tail}}$  (from Lemma C.1 and union bound), we note that on event  $A = \{\mathbf{y}_{1*} \in \mathcal{Y}_K \text{ and } \mathbf{y}_{2*} \in \mathcal{Y}_K\}$ , the error is zero. Thus, we add a conservative term for event  $B$ , where the error is at most  $2R_K^2(\mathbf{x})$  (since  $|\Delta_K|, |\Delta_\infty| \leq R_K(\mathbf{x})$ , so  $|\Phi_f^K(\mathbf{x}) - \Phi_f^\infty(\mathbf{x})| \leq 2R_K^2(\mathbf{x})$ ):

$$\begin{aligned} & \mathbb{E}[|\Phi_f^K(\mathbf{x}) - \Phi_f^\infty(\mathbf{x})| \cdot \mathbb{1}_B] \\ & \leq 2R_K^2(\mathbf{x}) \cdot \Pr(B) \leq 2R_K^2(\mathbf{x}) \cdot 2\varepsilon_{\text{tail}} = 4R_K^2(\mathbf{x})\varepsilon_{\text{tail}}, \end{aligned} \quad (88)$$

where  $\mathbb{1}_B$  is the indicator function which is 1 only when event  $B$  occurs.

Combining both terms, the expected error is:

$$\mathbb{E}[|\Phi_f^K(\mathbf{x}) - \Phi_f^\infty(\mathbf{x})|] \leq 2R_K^2(\mathbf{x}) \sqrt{\frac{2\pi}{K}} + 4R_K^2(\mathbf{x})\varepsilon_{\text{tail}}, \quad (89)$$

where  $\varepsilon_{\text{tail}} = (1 - P_f(\mathbf{y}_{1*}^K | \mathbf{x}))^K$ . This completes the proof.  $\square$

### C.8 Proof of Corollary 4.10

*Proof.* We aim to bound the tail probability  $\Pr(|\Phi_f^K(\mathbf{x}) - \Phi_f^\infty(\mathbf{x})| \geq \lambda)$  for  $\lambda > 0$ . Using the same notation as in Theorem 4.9, we have:

$$|\Phi_f^K(\mathbf{x}) - \Phi_f^\infty(\mathbf{x})| = |\Delta_K(\mathbf{x}) - \Delta_\infty(\mathbf{x})| \cdot |\Delta_K(\mathbf{x}) + \Delta_\infty(\mathbf{x})|. \quad (90)$$

Since  $|\Delta_K(\mathbf{x}) + \Delta_\infty(\mathbf{x})| \leq 2R_K(\mathbf{x})$ , let  $Z = |\Delta_K(\mathbf{x}) - \Delta_\infty(\mathbf{x})|$ , so:

$$|\Phi_f^K(\mathbf{x}) - \Phi_f^\infty(\mathbf{x})| \leq Z \cdot 2R_K(\mathbf{x}). \quad (91)$$

Thus:

$$\begin{aligned} & \Pr(|\Phi_f^K(\mathbf{x}) - \Phi_f^\infty(\mathbf{x})| \geq \lambda) \\ & = \Pr(Z \cdot 2R_K(\mathbf{x}) \geq \lambda) = \Pr\left(Z \geq \frac{\lambda}{2R_K(\mathbf{x})}\right). \end{aligned} \quad (92)$$

From the proof of Theorem 4.7 (Equation 50), Hoeffding's inequality gives:

$$\Pr(Z \geq t) \leq 4 \exp\left(-\frac{2Kt^2}{R_K^2(\mathbf{x})}\right). \quad (93)$$

Set  $t = \frac{\lambda}{2R_K(\mathbf{x})}$ :

$$\begin{aligned} & \Pr\left(Z \geq \frac{\lambda}{2R_K(\mathbf{x})}\right) \\ & \leq 4 \exp\left(-\frac{2K \cdot \left(\frac{\lambda}{2R_K(\mathbf{x})}\right)^2}{R_K^2(\mathbf{x})}\right) \\ & = 4 \exp\left(-\frac{K\lambda^2}{2R_K^4(\mathbf{x})}\right). \end{aligned} \quad (94)$$

Define events  $A = \{\mathbf{y}_{1*} \in \mathcal{Y}_K \text{ and } \mathbf{y}_{2*} \in \mathcal{Y}_K\}$  and  $B = \{\mathbf{y}_{1*} \notin \mathcal{Y}_K \text{ or } \mathbf{y}_{2*} \notin \mathcal{Y}_K\}$ . On event  $A$ , the error is zero, so it does not contribute to the tail probability. On event  $B$ , with  $\Pr(B) \leq 2\varepsilon_{\text{tail}}$  (from Lemma C.1 and union bound), the tail probability is bounded by:

$$\begin{aligned} & \Pr(|\Phi_f^K(\mathbf{x}) - \Phi_f^\infty(\mathbf{x})| \geq \lambda) \\ & \leq \Pr\left(\left\{Z \geq \frac{\lambda}{2R_K(\mathbf{x})}\right\} \cap B\right) + \Pr(A). \end{aligned} \quad (95)$$

Since  $\Pr(A) \geq 1 - 2\varepsilon_{\text{tail}}$  and the error is zero on  $A$ , we focus on event  $B$ :

$$\begin{aligned} & \Pr\left(\left\{Z \geq \frac{\lambda}{2R_K(\mathbf{x})}\right\} \cap B\right) \\ & \leq \Pr\left(Z \geq \frac{\lambda}{2R_K(\mathbf{x})}\right) + \Pr(B) \\ & \leq 4 \exp\left(-\frac{K\lambda^2}{2R_K^4(\mathbf{x})}\right) + 2\varepsilon_{\text{tail}}. \end{aligned} \quad (96)$$

Thus, the tail probability is:

$$\begin{aligned} & \Pr(|\Phi_f^K(\mathbf{x}) - \Phi_f^\infty(\mathbf{x})| \geq \lambda) \\ & \leq 4 \exp\left(-\frac{K\lambda^2}{2R_K^4(\mathbf{x})}\right) + 2\varepsilon_{\text{tail}}, \end{aligned} \quad (97)$$

where  $\varepsilon_{\text{tail}} = (1 - P_f(\mathbf{y}_{1*}^K | \mathbf{x}))^K$ . This completes the proof.  $\square$

## D Discussions

### D.1 Quantitative Analysis of Top-2 Sequence Similarity

As discussed in Section 4.3, the top two completions sampled under  $K$ -DPS can occasionally be nearly identical. We provide a quantitative assessment here. For all candidate sequences used to construct Figure 8, we measured the normalized Levenshtein edit distance between top-1 and top-2 completions.

Table 1: Average normalized edit distance between top-1 and top-2 completions as a function of  $K$ -DPS confidence score range.

$K$ -DPS Score Range	Avg. Normalized Edit Distance
< 0.1	0.15
< 0.5	0.20
< 1.0	0.23
< 5.0	0.30
< 10.0	0.32

As shown in Table 1, even in the highest-confidence regime ( $K$ -DPS < 0.1), the top-2 sequences differ by roughly 15% of tokens on average; near decision boundaries (higher  $K$ -DPS), divergence reaches 30–32%, confirming that the top two candidates are typically far from trivial variants.

## D.2 Effect of Filtering on the Local Candidate Set Bound

We next clarify whether token- or sequence-level filtering changes the theoretical guarantees. The answer depends on how filtering is used. If filtering is only a diagnostic or visualization post-processing step after computing the raw  $K$ -DPS, then none of the raw DPS theorems are changed. The quantities in Theorems 4.7–4.10 and Theorem 4.8 are still computed from the unfiltered language-model distribution  $P_f(\cdot|\mathbf{x})$ .

If filtering is used inside candidate selection, it should be viewed as defining a filtered or coarsened DPS variant. Let  $a_{\mathbf{x}}(\mathbf{y}) \in \{0, 1\}$  denote an acceptance rule for prompt  $\mathbf{x}$ , such as removing near-duplicate completions according to edit distance or a semantic-similarity threshold. The filtered candidate set is

$$\mathcal{Y}_K^a = \{\mathbf{y} \in \mathcal{Y}_K : a_{\mathbf{x}}(\mathbf{y}) = 1\}. \quad (98)$$

Assume that the top sequence is retained,  $a_{\mathbf{x}}(\mathbf{y}_{1*}) = 1$ , and define the accepted local near-second set

$$\mathcal{Y}_{2,\eta}^a(\mathbf{x}) = \{\mathbf{y} \in \mathcal{Y}^{N_r} : a_{\mathbf{x}}(\mathbf{y}) = 1, \mathbf{y} \neq \mathbf{y}_{1*}, \log P_f(\mathbf{y}|\mathbf{x}) \geq \log P_f(\mathbf{y}_{2*}|\mathbf{x}) - \eta\}. \quad (99)$$

Let

$$p_{2,\eta}^a(\mathbf{x}) = \sum_{\mathbf{y} \in \mathcal{Y}_{2,\eta}^a(\mathbf{x})} P_f(\mathbf{y}|\mathbf{x}) \quad (100)$$

be the probability mass of accepted candidates that are still within  $\eta$  nats of the raw second-best sequence.

The proof of Theorem 4.8 then applies without modification after replacing  $p_{2,\eta}(\mathbf{x})$  by  $p_{2,\eta}^a(\mathbf{x})$ . Specifically, on the event

$$E_\eta^a = \{\mathbf{y}_{1*} \in \mathcal{Y}_K^a\} \cap \{\mathcal{Y}_K^a \cap \mathcal{Y}_{2,\eta}^a(\mathbf{x}) \neq \emptyset\}, \quad (101)$$

the filtered sample still contains the raw top sequence and at least one accepted sequence whose log-likelihood is within  $\eta$  of  $\log P_f(\mathbf{y}_{2*}|\mathbf{x})$ . Hence

$$|\Phi_f^{K,a}(\mathbf{x}) - \Phi_f^\infty(\mathbf{x})| \leq \eta(2\Delta_\infty(\mathbf{x}) + \eta) \quad (102)$$

with probability at least

$$1 - (1 - P_f(\mathbf{y}_{1*}|\mathbf{x}))^K - (1 - p_{2,\eta}^a(\mathbf{x}))^K. \quad (103)$$

Thus, **filtering does not introduce any dependence on the global diameter  $R_K(\mathbf{x})$ . It only changes the candidate-discovery probability through the accepted local mass  $p_{2,\eta}^a(\mathbf{x})$ .** If the filter removes many near-second candidates, then  $p_{2,\eta}^a(\mathbf{x})$  decreases and a larger  $K$  may be needed; if the filter mainly removes low-probability duplicates or outliers far from the local top-2 band, the local bound is essentially unchanged.

There is one important distinction. If the filter deliberately removes the raw second-best sequence and all accepted candidates within  $\eta$  of it, then the estimator no longer targets the raw sequence-level DPS; it targets a coarsened semantic DPS. Let  $\mathbf{y}_{2*}^a$  be the best accepted non-top sequence and

$$\Delta_\infty^a(\mathbf{x}) = \log P_f(\mathbf{y}_{1*}|\mathbf{x}) - \log P_f(\mathbf{y}_{2*}^a|\mathbf{x}). \quad (104)$$

The same local candidate-set proof gives

$$|\Phi_f^{K,a}(\mathbf{x}) - \Phi_f^{\infty,a}(\mathbf{x})| \leq \eta(2\Delta_\infty^a(\mathbf{x}) + \eta), \quad (105)$$

where  $\Phi_f^{\infty,a}(\mathbf{x}) = (\Delta_\infty^a(\mathbf{x}))^2$ . Relative to the raw DPS, the only additional term is the intentional coarsening bias

$$|\Phi_f^{\infty,a}(\mathbf{x}) - \Phi_f^\infty(\mathbf{x})| = |\Delta_\infty^a(\mathbf{x})^2 - \Delta_\infty(\mathbf{x})^2|. \quad (106)$$

This term is not a sampling failure and is not controlled by  $R_K(\mathbf{x})$ ; it quantifies the deliberate change of target from raw sequence-level boundaries to filtered semantic boundaries. Consequently, filtering does not make the theoretical bound vacuous. It either leaves the raw local candidate-set bound intact, with  $p_{2,\eta}^a$  replacing  $p_{2,\eta}$ , or defines a separate coarsened DPS object with the same type of local bound plus an explicit coarsening bias relative to raw DPS.

## D.3 $K$ -DPS versus Model Uncertainty

We notice that the construction of explicit decision boundaries in the representation space might exhibit connections with several core research areas in LLMs, particularly confidence estimation and uncertainty quantification (UQ) (Geng et al. 2024; Huang et al. 2025; Liu et al. 2025b; Xia et al. 2025b; Shorinwa et al. 2025; Lin, Trivedi, and Sun 2024). These uncertainty quantification approaches typically include verbalized confidence expressed in natural language (Kadavath et al. 2022), token-level entropy of the output distribution (Kuhn, Gal, and Farquhar 2023), and semantic entropy computed over semantically equivalent clusters of multiple generations (Kuhn, Gal, and Farquhar 2023; Farquhar et al. 2024), with the latter achieving state-of-the-art performance in hallucination detection and selective generation tasks.

While these methods also measure the certainty and confidence of model decisions, our  $K$ -DPS decision-boundary construction differs from them in several fundamental aspects:

First, classical uncertainty quantification techniques (Kadavath et al. 2022; Kuhn, Gal, and Farquhar 2023; Farquhar et al. 2024) are essentially heuristic or sampling-based scores lacking formal theoretical guarantees, whereas  $K$ -DPS provides provably conservative classification boundaries with explicit error bounds. It achieves a precise and meaningful approximation of the decision boundary. Second, existing UQ methods operate at the instance level and treat each generation independently, while  $K$ -DPS explicitly builds and reasons over distribution-level decision boundaries, enabling global geometric understanding of the model’s reliable support. In terms of usage, conventional approaches remain largely oblivious to the location of samples relative to the empirical data manifold, whereas  $K$ -DPS deliberately identifies and penalizes anomalous boundary samples that fall near or outside the observed support of each semantic class. These distinctions shift the paradigm from post-hoc uncertainty scoring to principled, boundary-aware certification of LLM generations.

Nevertheless, we acknowledge that  $K$ -DPS and traditional uncertainty quantification methods indeed share some core insights. Both paradigms ultimately aim to identify when an

LLM’s output is unreliable, whether due to hallucination, out-of-distribution inputs, adversarial attacks, or memorization-based spurious responses. Technically, they all ground their analysis in the same internal representations of the model: prior UQ approaches directly use raw logits, token probabilities, or hidden states to compute verbalized confidence or entropy measures, whereas  $K$ -DPS leverages the DPF as the theoretical indicator to perform boundary construction. Consequently, the decision boundary learned by  $K$ -DPS can be interpreted as a geometrically principled extension of uncertainty signals: samples assigned high semantic entropy or low verbalized confidence often naturally fall into low-density or boundary regions detected by  $K$ -DPS, providing a unified explanatory framework for why existing UQ methods succeed or fail on specific examples. In practice, the two families of approaches are highly complementary: uncertainty scores can serve as lightweight pre-filters, while  $K$ -DPS offers stricter, certifiable analysis for LLM inference.

#### D.4 Effect of Sampling Temperature on DPS

We formalize the effect of temperature on the DPS. Recall that at each generation step  $t$ , the LLM produces a logit vector  $z^{(t)} \in \mathbb{R}^V$  from the hidden state, and the next-token distribution is obtained via softmax:  $P_f(y_t \mid \mathbf{x}, y_{<t}) = \text{softmax}(z^{(t)})_{y_t}$ . Let  $P_f^{(T)}(\mathbf{y} \mid \mathbf{x})$  denote the temperature-adjusted distribution with temperature  $T > 0$ , where the logits are scaled before softmax:  $P_f^{(T)}(y_t \mid \mathbf{x}, y_{<t}) = \text{softmax}(z^{(t)}/T)_{y_t}$ . The standard distribution is recovered at  $T = 1$ .

**Proposition D.1** (Monotonicity under Temperature). *For any prompt  $\mathbf{x}$  and temperature  $T_1 < T_2$ , the ordering of output sequences by log-probability is preserved. Consequently, the zero-height isohypse  $\mathcal{D}'_{(0,f)}$  is invariant under temperature changes, and the DPS undergoes a monotone transformation  $\Phi_f^{(\infty, T_2)}(\mathbf{x}) = \frac{1}{T_2^2} \Phi_f^{(\infty, T_1)}(\mathbf{x})$ .*

*Proof.* At temperature  $T$ , the log-probability of the generated token  $y_t$  at step  $t$  becomes  $\log P_f^{(T)}(y_t \mid \mathbf{x}, y_{<t}) = \frac{1}{T} z_{y_t}^{(t)} - \log Z_t^{(T)}$ , where  $Z_t^{(T)} = \sum_{v \in \mathcal{V}} \exp(z_v^{(t)}/T)$  is the per-step partition function. Summing over  $t = 1, \dots, N_r$  gives the sequence log-probability. Since  $z_{y_t}^{(t)}$  is independent of  $T$  and  $1/T > 0$  is strictly monotone, the ordering of sequences by log-probability is unchanged, so the identity of  $\mathbf{y}_{1*}$  and  $\mathbf{y}_{2*}$  is preserved. The DPF gap becomes  $\Delta_\infty^{(T)}(\mathbf{x}) = \frac{1}{T} \Delta_\infty^{(1)}(\mathbf{x})$ , yielding  $\Phi_f^{(\infty, T)}(\mathbf{x}) = \frac{1}{T^2} \Phi_f^{(\infty, 1)}(\mathbf{x})$ .  $\square$

Proposition D.1 implies that temperature scales the DPS values by  $1/T^2$  while preserving the zero-height isohypse. Higher temperature compresses the surface vertically, reducing the dynamic range of DPS values; lower temperature amplifies differences. In both cases the topological structure of isohypses, including the decision boundary itself, remains identical.

#### D.5 Sampling Strategies and DPS

In practice, candidate sequences  $\mathcal{Y}_K$  are drawn using decoding strategies rather than the raw model distribution. We discuss the compatibility of common strategies with  $K$ -DPS.

- **Nucleus (top- $p$ ) sampling** restricts candidates to the smallest set whose cumulative probability exceeds  $p$ . Since this set is a subset of the support of  $P_f$ , the error bounds in Theorems 4.7–4.10 remain valid, with  $\varepsilon_{\text{tail}}$  now depending on the truncated distribution. For typical  $p \in [0.9, 0.95]$ , the truncation is mild and the bounds hold with slightly adjusted constants.

- **Top- $k$  sampling** restricts candidates to the  $k$  most likely tokens at each step. When  $k \ll V$ , the sampling distribution differs from  $P_f$ , and the theoretical bounds require modification to account for the restricted support. However, we recommend  $k$  large enough (e.g.,  $k \geq 50$ ) so that the top few tokens at each step are always included, which is sufficient for accurate DPS estimation at modest  $K$ .

- **Temperature** affects the sampling distribution as analyzed in Appendix D.4. When temperature is used only for candidate generation while evaluating DPF values on the raw ( $T = 1$ ) logits, the theoretical guarantees apply directly. When temperature is applied to both generation and evaluation, Proposition D.1 guarantees that the decision boundary structure is preserved.

Note that the above comparison is about the DPS between the standard token sampling and these sampling strategies. If we consider the sampling strategy itself as part of the model, then the above analysis is unnecessary and the original derivations still apply.

In our experiments (Section 5) we use nucleus sampling with  $p = 0.9$  and evaluation on raw logits, which balances sample diversity with theoretical fidelity.

### E Additional Empirical Analysis

We provide supplementary empirical checks for the stability of  $K$ -DPS estimation. These results address five practical factors that could affect the estimator: model scale, the normalization of the estimation error, the maximum decoding length, the sampling strategy, and the model family.

#### E.1 Model-Size Ablation

We first test whether the sample budget needed for stable  $K$ -DPS estimation changes substantially with model size. We evaluate the Pythia Biderman et al. (2023) family, from 70M to 1.4B parameters, on the AdvBench harmful-prompt set. For each model, we compute the absolute difference between the  $K$ -DPS estimate and a reference estimate computed with  $K = 2,500$ , while varying the sampling budget from  $K = 500$  to  $K = 1,250$ .

Table 2 shows that the estimator stabilizes across all tested model sizes. Once  $K \geq 1,000$ , the discrepancy from the  $K = 2,500$  reference estimate is below  $10^{-13}$ , i.e., at numerical precision. The smaller-budget columns also show a consistent trend: larger models tend to have lower error at the same  $K$ . This is consistent with the top completions carrying more concentrated probability mass, which makes the top-2 gap easier to recover from samples.

Table 2: Estimation error of  $K$ -DPS across Pythia model scales. Reference  $K = 2,500$ . Errors below  $10^{-13}$  are at machine precision.

Model	$K=500$	$K=750$	$K=1,000$	$K=1,250$
70M	240.91	105.86	$1.17 \times 10^{-14}$	$1.17 \times 10^{-14}$
160M	212.16	90.98	$1.38 \times 10^{-14}$	$1.38 \times 10^{-14}$
410M	213.60	99.94	$9.33 \times 10^{-15}$	$9.33 \times 10^{-15}$
1B	155.98	65.48	$8.63 \times 10^{-15}$	$8.63 \times 10^{-15}$
1.4B	160.97	66.93	$1.12 \times 10^{-14}$	$1.12 \times 10^{-14}$

## E.2 Relative Error Ratio

Absolute error alone can be hard to interpret when the reference DPS values vary in magnitude. We therefore also examine the relative error ratio  $|\Phi_f^K(\mathbf{x}) - \Phi_f^{20,000}(\mathbf{x})| / (\Phi_f^{20,000}(\mathbf{x}) + \epsilon)$ , with  $\epsilon = 10^{-8}$ . This metric measures the estimation error relative to the scale of the reference value and is therefore complementary to the absolute-error curves in the main text.

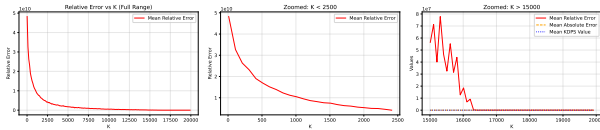


Figure 12: Relative error ratio of  $K$ -DPS as a function of the sampling budget  $K$ . The reference value is computed with  $K = 20,000$ .

Figure 12 shows that the relative error decreases rapidly with  $K$  and is already close to zero before  $K = 2,500$  on the examined inputs. The trend is consistent with the  $1/\sqrt{K}$  convergence rate predicted by Theorem 4.7. Thus the convergence is not an artifact of using an absolute scale: the estimator is also accurate relative to the magnitude of the DPS value itself.

## E.3 Long-Generation Tail Probability and Length Budget

We next clarify the role of generation length in the tail-probability term. The main issue is not the vocabulary size alone, but the joint probability of an exact generated sequence. For very long, high-entropy generation, this joint probability can be small even when the model assigns high probability to most individual tokens. To make this point explicit, we evaluated top-1 sequence probabilities under an 8K-token maximum decoding setting on long-form reasoning and generation prompts.

Table 3 supports a more precise reading of the theory. In long open-ended settings, the sequence-level top-1 probability can indeed be very small: for example, the mean top-1 sequence probability for Llama-3.1-8B is  $5.86 \times 10^{-13}$ . This means that the original tail-probability bound may require a much larger sample budget if it is interpreted as a guarantee for exact 8K-token sequence recovery. This is a limitation of exact sequence-level boundary construction in high-entropy generation, and we state it explicitly.

Table 3: Top-1 sequence probability under an 8K-token decoding cap. The cap is the maximum allowed length; the realized generation length can be shorter.

Model	Avg. Len.	Mean Top-1 Seq. Prob.	Avg. Token Prob.
Llama-3.1-8B	7505	$5.86 \times 10^{-13}$	0.967
Llama-3.2-3B	3572	$1.44 \times 10^{-3}$	0.856
Qwen3.5-9B	1913	$8.45 \times 10^{-3}$	0.892
Qwen2.5-7B	6058	$7.14 \times 10^{-5}$	0.938

At the same time, **these numbers should not be interpreted by dividing the log sequence probability by the maximum cap of 8K tokens in every case.** The cap is not the realized length: the average realized lengths in Table 3 range from 1913 to 7505 tokens. Moreover, the average per-token probabilities remain moderate to high. The small joint probabilities arise from multiplying many token probabilities over long outputs, not from every token having an implausibly tiny probability. This highlights the practical scope of exact sequence-level DPS: its sampling guarantee is most meaningful when the relevant top sequences have non-negligible probability mass, whereas very long high-entropy completions are better analyzed through localized or prefix-conditioned variants.

For this reason, our empirical  $K$ -DPS claims are intended for the bounded-length response regimes studied in the main experiments. In very long open-ended generation, token-level DPS (Section 4.3,  $N_r = 1$ ), prefix-conditioned DPS, or shorter-window sequence DPS is the appropriate diagnostic because the candidate mass is concentrated locally at each prefix rather than over an entire 8K-token completion.

**Bounded-length ablation.** As a separate sanity check, we also vary a moderate maximum generation length from 16 to 256 tokens using Llama-3.2-1B on Wikipedia Mini. Table 4 reports the resulting  $K$ -DPS values and absolute errors relative to the corresponding high-budget reference estimator.

Table 4: Effect of maximum generation length on  $K$ -DPS estimation. The length column is the decoding cap, not the average realized generation length.

Max. Length	$K$ -DPS Value	Abs. Error
16	0.002	$\approx 0$
32	0.72	$\approx 0$
64	0.66	$\approx 0$
128	0.29	$\approx 0$
256	0.41	$\approx 0$

Within this bounded-length range, increasing the maximum length does not cause a systematic increase in estimation error. This experiment therefore supports the stability of  $K$ -DPS for the response lengths used in our main empirical studies, but it should not be read as a claim that the same sample budget resolves arbitrary 8K-token open-ended generation.

#### E.4 Sampling-Strategy Sensitivity

We finally test whether the estimator depends on the decoding strategy used to construct the candidate set. Table 5 summarizes the comparison.

Table 5: Effect of sampling strategy on  $K$ -DPS estimation. Greedy search is degenerate for  $K$ -DPS because it repeatedly returns a single candidate and therefore cannot estimate a top-2 sample gap.

Sampling Strategy	$K$ -DPS Value	Abs. Error
Greedy search	–	–
Nucleus sampling	0.144	$\approx 0$
Top- $k$ clipping	0.25	$\approx 0$

Greedy search is degenerate for this purpose: repeated decoding returns the same highest-probability sequence, so the sample set does not contain the second candidate needed to estimate a top-2 gap. Stochastic strategies such as nucleus sampling and top- $k$  clipping avoid this collapse by preserving candidate diversity. Under the same likelihood evaluation protocol, both stochastic strategies produce essentially zero absolute error against the reference estimate, supporting our use of stochastic candidate generation followed by raw-logit likelihood evaluation.

## F Visualization Details

While this paper primarily focuses on the error analysis of LLM decision boundary construction, our proposed  $K$ -DPS can also be used to intuitively visualize both the decision boundary and the decision potential surface of an LLM under a given input distribution, as detailed in Section 5.4. In this section, we detail the settings and the visualization effectiveness.

**Settings.** For visualization, we construct a low-dimensional representation of the original input distribution  $\mathcal{D}'$ , typically in two dimensions to facilitate human understanding. First, we extract the last hidden state of an input  $\mathbf{x}$  from the LLM as the original embedding of the input point. Next, we apply UMAP with 100 neighbors and a minimum distance of 0.2 for dimensionality reduction. Finally, we normalize the reduced embeddings to the range  $[0, 1]$  to construct the decision potential surface visualization. For interpolation, we evaluate nearest, linear, and cubic interpolation methods to approximate the  $K$ -DPS values on a mesh grid.

**Role of Projection.** We emphasize that dimensionality reduction (UMAP) is used *only for visualization*; all quantitative conclusions in this paper are based on the  $K$ -DPS values computed at **actual** input data points **without** any projection. The interpolation over the mesh grid visualizes the surface, but the numerical claims about convergence, error, and boundary structure are drawn directly from the sample-level DPF values. To further validate that the observed trends are not artifacts of UMAP, we provide visualizations with three complementary interpolation methods (nearest, linear, cubic) in Figures 6, 8, and 9, respectively. The nearest and linear interpolations preserve the sign and monotonicity of observed  $K$ -DPS values in all regions, and the consistent boundary

structures across all three methods confirm that the qualitative results are robust to the choice of interpolation. Cubic interpolation may produce slight negative values in sparse regions (e.g., top-left quadrants of some panels in Figure 6), which are interpolation artifacts from the absence of input samples in those areas, not errors in the underlying  $K$ -DPS computation.